

INVESTIGATION OF IN VITRO CYTOTOXIC EFFECTS OF HEPARIN
COATED IRON OXIDE NANOPARTICLES COMBINED WITH TPP-DCA ON
HUMAN HEPATOCELLULAR CARCINOMA CELL LINE HEPG2

A THESIS SUBMITTED TO
THE GRADUATE SCHOOL OF NATURAL AND APPLIED SCIENCES
OF
MIDDLE EAST TECHNICAL UNIVERSITY

BY

BAŞAK EZGİ SARAÇ

IN PARTIAL FULFILLMENT OF THE REQUIREMENTS
FOR
THE DEGREE OF MASTER OF SCIENCE
IN
BIOLOGY

JUNE 2018

Approval of the thesis:

**INVESTIGATION OF IN VITRO CYTOTOXIC EFFECTS OF HEPARIN
COATED IRON OXIDE NANOPARTICLES COMBINED WITH TPP-DCA
ON HUMAN HEPATOCELLULAR CARCINOMA CELL LINE HEPG2**

submitted by **BAŐAK EZGİ SARAÇ** in partial fulfillment of the requirements for the degree of **Master of Science in Biological Sciences Department, Middle East Technical University** by,

Prof. Dr. Halil Kalıpçılar
Dean, Graduate School of **Natural and Applied Sciences**

Prof. Dr. Orhan Adalı
Head of Department, **Biological Sciences**

Prof. Dr. N. Tülin Güray
Supervisor, **Biological Sciences Dept., METU**

Examining Committee Members:

Prof. Dr. Orhan Adalı
Biological Sciences Dept., METU

Prof. Dr. N. Tülin Güray
Biological Sciences Dept., METU

Assoc. Prof. Dr. Çağdaş Devrim Son
Biological Sciences Dept., METU

Prof. Dr. Mürvet Volkan
Chemistry Dept., METU

Prof. Dr. Özlem Yıldırım
Biological Dept., Ankara University

Date: 29/06/2018

I hereby declare that all information in this document has been obtained and presented in accordance with academic rules and ethical conduct. I also declare that, as required by these rules and conduct, I have fully cited and referenced all material and results that are not original to this work.

Name, Last name: BAŐAK EZGİ SARAÇ

Signature:

ABSTRACT

INVESTIGATION OF IN VITRO CYTOTOXIC EFFECTS OF HEPARIN COATED IRON OXIDE NANOPARTICLES COMBINED WITH TPP-DCA ON HUMAN HEPATOCELLULAR CARCINOMA CELL LINE HEPG2

Saraç, Başak Ezgi

M.Sc., Department of Biology

Supervisor: Prof. Dr. N. Tülin Güray

Co-supervisor: Prof. Dr. Mürvet Volkan

June 2018, 68 pages

Nanotechnology in medicine involves the applications of nanoparticles and one of the rising field is cancer nanotechnology, which has been increasingly used in cancer diagnostics, imaging, and therapeutic drug delivery. The advantage of the use of the nanoparticles is that, they can be designed to be specific for tumor tissue. This allows increased drug delivery efficiency and reduced off-target toxicities. Iron oxide nanoparticles used in this study are smaller than 100 nm but still it gives an enhanced surface area for the delivery of drugs.

Considering the tumor metabolism, targeted therapeutic agents are an alternative anti-tumor treatment which has wide potentials. In most cancer cells, fast growing is related to the disabled mitochondria and consequently cells resist to undergo apoptosis and able to grow in the absence of oxygen.

Dichloroacetate (DCA) which is a pyruvate dehydrogenase kinase inhibitor, reverse this process, reduce proliferation and inhibit the tumor growth. However, the DCA dose required to show this effect is significantly high. In order to use a pharmacologically suitable dose, magnetic nanoparticles which can increase the cellular uptake of DCA can be a more efficient alternative. Therefore, in this study, iron oxide nanoparticles (Fe_3O_4) were first modified with heparin, Dichloroacetate (DCA) is placed inside the heparin layers and in order to use glucose channels, conjugated with 2-deoxy-D-glucose. Triphenylphosphonium (TPP) was also added to induce the uptake by mitochondria. Internalization of nanoparticles, their cytotoxicity, effects on mitochondrial membrane potential and apoptotic pathways were further analyzed in human hepatocellular carcinoma cell line, HepG2.

Uptake assays performed with naked nanoparticles, 1-layer heparin coated TPP-DCA conjugated 2-DG attached nanoparticles, and nanoparticles with 2-layer heparin coated TPP-DCA conjugated with or without 2-DG showed that, heparin coating and 2-DG conjugation significantly increased cellular uptake of particles. Cytotoxicity experiments showed that, tailored nanoparticles increased DCA delivery into cancer cells compared to commercially available Na-DCA drug even when it was conjugated to triphenylphosphonium (TPP). Apoptosis studies indicated that tailored nanoparticles drive cells to undergo apoptosis rather than necrosis. Also, they decreased mitochondrial membrane potential, shifting the hyperpolarization to depolarization indicating that, 2-layer heparin coated TPP-DCA conjugated 2-DG attached nanoparticles not only increased DCA delivery significantly, but also killed hepatocellular carcinoma, HepG2 cells through apoptosis.

Keywords: Dichloroacetate, triphenylphosphonium, iron oxide nanoparticles, 2-D Glucose, liver cancer, drug delivery

ÖZ

HEPARİN İLE KAPLANIP TPP-DKA İLE KONJUGE EDİLMİŞ DEMİR OKSİT NANOPARÇACIKLARININ İNSAN KARACİĞER KANSER HÜCRE HATTI ÜZERİNDEKİ ETKİSİNİN İN VİTRO ARAŞTIRILMASI

Saraç, Başak Ezgi

Yüksek Lisans, Biyoloji Bölümü

Tez Yöneticisi: Prof. Dr. N. Tülin Güray

Ortak Tez Yöneticisi: Prof. Dr. Mürvet Volkan

Haziran 2018, 68 sayfa

Tıpta nanoteknoloji, nanoparçacıkların uygulamalarını içeren kanser biyoteknolojisinin yükselen alanlarından biri olup, kanser teşhisi, görüntüleme ve terapötik ilaç gönderimi alanlarında giderek daha çok kullanılmaktadır. Nanoparçacık kullanımının avantajlarından biri tümör dokusuna göre spesifik olarak dizayn edilebilmesidir. Bu özelliği ile ilaç gönderimindeki verimin artırılmasına katkı verirken hedef dışı toksisitenin azalmasını da sağlamaktadır. Bu çalışmada kullanılan demir oksit nanoparçacıklarının boyutu 100 nm'den küçük olmasına rağmen ilaç gönderimi için büyük yüzey alanı oluşturmaktadır.

Tümör metabolizması göz önünde bulundurulduğunda hedeflenmiş terapötik ajanlar tümör tedavisinde potansiyel alternatiflerdir. Çoğu kanser hücresinde hızlı çoğalma apoptoza direnme ve oksijen yokluğunda dahi büyümeye olanak sağlayan işlevi bozulmuş mitokondriler ile ilişkilendirilmiştir.

Bir pirüvat dehidrogenaz kinaz inhibitörü olan dikloroasetat (DKA) bu süreci tersine çevirerek proliferasyonu azaltmakta ve tümör büyümesini engellemektedir. Ancak, DKA'nın bu etkiyi gösterebilmesi için gereken doz çok yüksektir. Farmakolojik olarak uygun dozu kullanabilmek için DKA'nın hücre alımını artırabilecek manyetik nanoparçacıklar daha etkili bir alternatif olarak karşımıza çıkmaktadır. Bu sebeple bu çalışmada, demir oksit nanoparçacıkları (Fe_3O_4) önce heparin ile modifiye edilmiş, dikloroasetat (DKA) heparin katmanları arasına yerleştirilmiş ve glikoz kanallarını kullanarak hücre içine girebilmesi için 2-D Glucose ile konjüge edilmiştir. Ayrıca mitokondriyal alımı artırmak için DKA trifenilfosfonyum (TPP) ile bağlanmıştır. Nanoparçacıkların hücre içine alımı, sitotoksiteleri, mitokondriyal membran potansiyeli ve apoptotik yollar üzerine etkileri insan hepatoselüler karsinoma hücre hattı olan HepG2 üzerinde analiz edilmiştir.

Çıplak nanoparçacık, 1 kat heparinle kaplanmış TPP-DKA ile konjüge edilip 2-DG bağlanan nanoparçacıklar ile 2 kat heparinle kaplanmış TPP-DKA ile konjüge edilip 2-DG ile bağlanan ve bağlanmayan nanoparçacıklar ile gerçekleştirilen hücre alım deneylerinin sonucunda heparin kaplamanın ve 2-DG konjügasyonunun nanoparçacıkların hücre içine alımını kayda değer miktarda artırdığı gözlemlenmiştir. Sitotoksite sonuçlarına göre, hazırlanan nanoparçacıklar ticari olarak satılan Na-DKA ilacına oranla kanser hücrelerine DKA gönderimini artırmıştır. Apoptotik etkilerini değerlendirmek amacıyla yapılan apoptoz deneyinden elde edilen sonuçlar hazırlanan nanoparçacıkların kanser hücrelerini nekroz yerine apoptoza sürüklediğini göstermiştir.

Bunun yanısıra, kullanılan nanoparçacık ürünü mitokondri membranını hiperpolarizasyondan depolarizasyona kaydırarak mitokondriyel membran potansiyelini yüksek miktarda azaltmış ve 2 kat heparinle kaplanmış TPP-DKA ile konjüge edilip 2-DG bağlanan nanoparçacıklar yalnızca DKA gönderimini artırmamış, aynı zamanda hepatoselüler karsinoma hücre hattı olan HepG2 hücrelerinin apoptoz yoluyla ölümüne neden olmuştur.

Anahtar Kelimeler: Dikloroasetat, trifenilfosforyum, demir oksit nanoparçacıkları, karaciğer kanseri, ilaç gönderimi

Dedicated to my family and my love,

ACKNOWLEDGEMENTS

This thesis is a result of the support and guidance I have received from numerous people throughout my graduate study. It is a great pleasure to have this opportunity to express my deep sense of gratitude.

First and foremost, I would like to thank Prof.Dr. N. Tülin Güray for her endless guidance, support, motivation and trust throughout my study. She always supported me and encouraged me when I felt desperate. She gave me all the time and help I needed during this study without any complain and helped me to improve myself in order to be a good researcher. Her great effort made this thesis possible. It was big honor to work with her.

I would like to thank my co-supervisor, Prof. Dr. Mürvet Volkan for her sincere guidance, valuable suggestions and encouragement. She has always kept her faith in me, even when I could not. I really appreciate her support and trust.

I would like to express my great gratitude to Dr. Yeliz Akpınar for her sincere guidance and priceless friendship. She was like a big sister for me and helped me in every obstacle I faced during this study. She has worked day and night to prepare nanoparticles for me to complete my study in time. Without her inspiring advices and encouragement, I couldn't complete the thesis.

I would like to express my sincere appreciation to İhsan Cihan Ayanoglu for helping me in flow cytometry assays. I am very grateful to work with him.

I would like to thank Assoc.Prof.Dr. Çağdaş Devrim Son for his valuable suggestions and guidance throughout this study especially in fluorescence experiments.

I also thank the members of the thesis committee Prof. Dr. Orhan Adalı and Prof.Dr. Özlem Yıldırım for their valuable time, suggestions and assistance.

I would like to thank Assist. Prof. Dr. Deniz İrtem Kartal for her guidance when I was a special project student.

I would also like to thank Elif Sakallı, Zeynep Eda Akyıldız and Dilara Koç for their support and friendship.

I would like to thank to members of Prof.Dr. Mürvet Volkan's laboratory; Pakizan Tasman, Merve Nur Güven, Begüm Avcı for their friendship during this study.

My sincere gratitude goes to my best friends for their endless support, motivation and support. My special thank goes to İpek Özyurt for being such a good friend and colleague and her immense support. She was always -literally- there for me for every trouble as well as the fun times. I could not stop smiling when I remember the moments with her. I would also thank my oldest friend, Deniz Kara for making me feel so lucky to have her in my life. My deepest appreciation goes to Seçil Aluç for her priceless friendship. She is one of the few people who I know with such a great personality. She, in any case, was there when I needed her.

My deepest thanks and gratitude go to my family, especially my mother, Fatma Saraç without whom I would not be able to get where I am now and my father, Sinan Saraç for their endless love and support not only during my graduate study but also in all stages of my life. I would also thank my brother, Ertan Saraç, my sister-in-law, Damla Doğan Saraç and my precious little niece, Fatma Hazal Saraç for being there for me all the time. There is no way I can appreciate my uncle-in-law who is more than a father to me, Dr.Vural Dirimeşe, my aunts, Aydanur Saraç, Atanur Saraç and my cousin, Edanur Saraç for their immense support and love.

Last but certainly not least, I cannot express my deep feelings in words towards my love, Emrah Sandıkçı. I am grateful for his support, motivation, friendship, love and that persistent attitude that never left me alone. He always believed in me and encouraged me to go forward and pursue my dreams. I always feel like the luckiest person in the world to have him in my life. He has been with me during the hard as well as the cheerful times.

I also wish to thank all in Biological Sciences and Chemistry Department of METU.

TABLE OF CONTENTS

ABSTRACT.....	v
ÖZ.....	vii
ACKNOWLEDGEMENTS.....	xii
TABLE OF CONTENTS.....	xvii
LIST OF TABLES.....	xxi
LIST OF FIGURES.....	xxiii
LIST OF ABBREVIATIONS.....	xxvi
CHAPTERS	
1. INTRODUCTION.....	1
1.1 Cancer.....	1
1.2 Liver Cancer.....	2
1.3 Treatment Strategies for Liver Cancer.....	2
1.3.1 Chemotherapy for Liver Cancer.....	3
1.3.2 Dichloroacetate as Anti-Cancer Drug.....	3
1.3.2.1 New approach for DCA delivery	5
1.4 Nanobiotechnology in cancer and drug delivery	5
1.4.1 Nanoparticles	8
1.4.1.1. Iron Oxide Nanoparticles	9
1.4.1.2 Surface Modifications	9
1.4.1.3 2-layer Heparin Coated TPP-DCA conjugated 2-D- Glucose Attached Iron Oxide Nanoparticles	11
1.5 Aim of the Study.....	12

2. MATERIALS AND METHODS.....	13
2.1 Materials.....	13
2.2 Methods.....	14
2.2.1 Preparation of Nanoparticles.....	14
2.2.2 Cell Culture.....	16
2.2.2.1 Cell Culture Conditions and Medium.....	16
2.2.2.2 Treatments.....	16
2.2.2.3 Cell Seeding.....	17
2.2.2.4 Cell Growth and Passaging.....	17
2.2.2.5 Cell Freezing.....	18
2.2.2.6 Cell Counting.....	18
2.2.3 Cytotoxicity Assays.....	20
2.2.3.1 XTT Cell Proliferation Assay.....	20
2.2.3.2 Trypan Blue Exclusion Method.....	22
2.2.4. Visualization of Cells Treated with Nanoparticles.....	23
2.2.5 Determination of Cellular Uptake of Nanoparticles.....	23
2.2.6 Annexin V-FITC Apoptosis Assay.....	25
2.2.7 Detection of Mitochondrial Membrane Potential via JC-10 Assay...	26
3. RESULTS AND DISCUSSION.....	27
3.1 Preparation and Optimization of Nanoparticles.....	27
3.2 Cell Culture.....	28
3.2.1 Cytotoxicity Assays.....	28

3.2.1.1 XTT Cell Proliferation Assay	28
3.2.1.2 Trypan Blue Exclusion Method	35
3.2.2 Visualization of Cells by Light Microscopy	37
3.2.3 Determination of Cellular Uptake of Nanoparticles	43
3.2.4 Annexin V-FITC Apoptosis Assay	48
3.2.5 Mitochondrial Membrane Potential Assay	51
4. CONCLUSION	53
REFERENCES	55

LIST OF TABLES

TABLES

Table 3.1 Inhibitory concentrations of 2-L-H TPP-DCA 2-DG NPs on HepG2 cell growth.....	33
---	----

LIST OF FIGURES

FIGURES

Figure 1.1 Chemical structure of sodium dichloroacetate (Na-DCA).....	4
Figure 1.2 Metabolic differences in normal and cancer cells and tissues. OXPPOS refers to oxidative phosphorylation. (Kalyanaraman, 2017).....	6
Figure 1.3 Chemical structure of heparin.....	11
Figure 2.1 Preparation of heparin coated iron oxide nanoparticles conjugated with TPP-DCA. A) Heparin coating, B) TPP-DCA conjugation, C) Additional heparin coating.....	15
Figure 2.2 (A) Hemocytometer chamber, (B,C) Counting technique.....	19
Figure 2.3 Formation of XTT tetrazolium to XTT formazan product.....	20
Figure 2.4 Representative template of 96-well plate showing the treatment pattern. DC: DMSO Control.....	22
Figure 2.5 Representation of increase in cell granularity in response to cellular uptake of the cell. While cell size remain constant, granularity/complexity of the cell increases with the exposure of NPs.....	24
Figure 3.1 TEM image and size distribution of A) Iron oxide nanoparticles (Naked nanoparticles), B) heparin coated iron oxide nanoparticles, C) 2-DG-HEP-TPP-DCA-HEP coated IONPs or 2-L-H TPP-DCA 2-DG NPs.....	27

Figure 3.2 The effects of Na-DCA and TPP-DCA on HepG2 cell growth by using XTT assay. The viability of cells was represented as cell viability percentages, means \pm SEM.....	30
Figure 3.3 XTT Assay results without magnetic wash	31
Figure 3.4 XTT Assay results of naked nanoparticles. The viability of cells was represented by cell viability percentages as means \pm SEM.....	32
Figure 3.5 XTT Assay results of two-layer heparin coated, 2-D Glucose conjugated iron oxide nanoparticles with or without TPP-DCA. The viability of cells was represented by cell viability percentages as means \pm SEM.....	33
Figure 3.6 Inhibitory effects of 2-L-H TPP-DCA 2-DG NPs on HepG2 cell growth calculated by using XTT Assay. The viability of cells was represented by cell viability percentages as means \pm SEM.....	34
Figure 3.7 Cell counts after 24hr treatment with 5 different samples at concentrations of 250 and 500 $\mu\text{g/mL}$	36
Figure 3.8 Comparison of cell viability treated with two-layer heparin coated nanoparticles with or without TPP-DCA at three different concentrations of 250, 500, and 1000 $\mu\text{g/mL}$	37
Figure 3.9 Comparison of microscope images of cells treated with one-layer heparin NPs and two-layer heparin NPs.....	39
Figure 3.10 Comparison of microscope images of cells treated with naked NPs and two-layer heparin coated TPP-DCA conjugated 2-DG attached NPs.....	40

Figure 3.11 Comparison of microscope images of cells treated with two-layer heparin coated TPP-DCA conjugated 2-DG attached NPs with or without magnetic wash...41

Figure 3.12 Images of 4 different nanoparticle products (A) Immediately after ultrasonication, (B) 15 minutes after ultrasonication.....42

Figure 3.13 Images of wells containing 4 different nanoparticle products after 24-hour treatment before washing.....43

Figure 3.14 Uptake of different nanoparticle products by HepG2 cell line. Real images after treatments with different concentration of NPs (50, 285 and 500 $\mu\text{g}/\text{mL}$) are shown for 24 h and given in the flow cytometry histograms.....45

Figure 3.15 The histograms of the apoptotic effects of 2-DG-HEP-TPP-DCA-HEP coated IONPs at concentrations of 285 $\mu\text{g}/\text{mL}$ and 525 $\mu\text{g}/\text{mL}$ on HepG2 cells. Bar graphs show percent apoptotic cells. DMSO control (DC) was used as negative control and 16 hr 50 μM etoposide exposure was used as positive control. Four subpopulations and their percent distributions in different areas: Area A1 shows viable cells while A3 represents dead cells (necrotic). A2 and A4 correspond to early and late apoptotic events, respectively.....47

Figure 3.16 The histograms of the apoptotic effects of 2-DG-HEP-TPP-DCA-HEP coated IONPs at concentrations of 285 $\mu\text{g}/\text{mL}$ and 525 $\mu\text{g}/\text{mL}$ on HepG2 cells. Bar graphs show percent apoptotic cells. DMSO control (DC) was used as negative control and 16 hr 50 μM etoposide exposure was used as positive control. Four subpopulations and their percent distributions in different areas: Area A1 shows viable cells while A3 represents dead cells (necrotic). A2 and A4 correspond to early and late apoptotic events, respectively.....49

Figure 3.17 The histograms of the mitochondrial membrane potential change in cells treated with 2-DG-HEP-TPP-DCA-HEP coated IONPs at concentrations of 285 $\mu\text{g}/\text{mL}$ and 525 $\mu\text{g}/\text{mL}$ on HepG2 cells. DMSO control (DC) was used as negative control and cells treated with 8.7 μM CCCP were used as positive control. Two subpopulations and their percent distributions in different areas: Area A1 shows hyperpolarization while A2 represents depolarization in mitochondrial membrane...51

LIST OF ABBREVIATIONS

2-DG	2-deoxyglucose
ATCC	American Type Culture Collection
CCCP	Carbonyl cyanide 3-chlorophenylhydrazone
DCA	Dichloroacetate
DMEM	Dulbecco's Modified Eagle's medium
DMSO	Dimethylsulfoxide
DOX	Doxorubicin
ERK	Extracellular signal-regulated kinase
FBS	Fetal bovine serum
FITC	Fluorescein
FSC	Forward-scattered
GA-MNPs	Glucosaminic acid-modified magnetic nanoparticles
GLUT	Glucose transporter
GLUT1	Glucose transporter 1
HCC	Hepatocellular carcinoma
IC50	Inhibitory concentration to kill 50% of the population
IONPs	Iron oxide nanoparticles
MNPs	Magnetic nanoparticles
Na-DCA	DCA conjugated with sodium salt
NP	Nanoparticle

OXPPOS	Oxidative phosphorylation
PBS	Phosphate buffered saline
PDH	Pyruvate dehydrogenase
PDK1	Pyruvate dehydrogenase kinase 1
Pen-Strep	Penicillin-Streptomycin
PI	Propium Iodide
Pn-SPIONs	Pullulan supermagnetic iron oxide nanoparticles
PS	Phosphatidylserine
ROS	Reactive oxygen species
SSC	Side-scattered
TACE	Chemotherapeutic drugs and embolic particles
TAE	Embolic particles without chemotherapy
TEM	Transmission Electron Microscopy
TPP	Triphenylphosphonium
TPP-DCA	TPP conjugated with DCA
XRD	X-Ray Diffraction
XTT	2,3-Bis-(2-Methoxy-4-Nitro-5-Sulfophenyl)-2H-Tetrazolium-5-Carboxanilide

CHAPTER 1

INTRODUCTION

1.1 Cancer

Cancer is a general definition for a broad group of diseases in which cells undergo an uncontrolled cell division and invasion. In healthy organisms, almost all cells except cells belong to muscles and nervous system are capable of dividing in a controlled manner to replace dead cells and repair damaged or wounded tissues, although their ability to do so are restricted to a certain extent. On the other hand, cancer cells that may originate from anywhere of the body grow abnormally in an uncontrolled fashion and eventually spread and invade other tissues and organs, a process termed metastasis (Fidler *et.al.*, 2015). Normally, a balance between cell proliferation and apoptosis that is also referred as cell turnover maintains homeostasis within the tissues and organs (Bertram, 2000). Even small disruptions in this process resulted from any genetic changes due to mutations or other events break this balance and cause cells to behave abnormally which may eventually give rise to generation of cancerous cells. Tumor cells are usually classified into two main categories according to their properties as benign and malignant. Although benign tumors can grow to form a large mass that may apply pressure on neighboring tissues, they lack the ability to spread or invade other tissues and organs by leaking through lymphoid or blood vessels, whereas malignant tumors can do. Cancer types are named based on the place they originate, such as breast, lung, colorectal, and liver cancer and they show different growth rates and metastatic properties. Therefore, strategies used to treat each cancer type are different, since different cancer types will not respond the same treatment in the same way. Cancer is one of the primary reasons of death worldwide. According to recent statistics reported in 2018 (Siegel, 2018), only in United States, there are 1,735,350 new cancer cases and 609,640 cancer deaths.

1.2 Liver Cancer

According to statistics reported in 2018, liver cancer is one of the most common cancer type and its occurrence continues to increase in females, while remains constant in males (Siegel, 2018; American Cancer Society, 2018). Liver cancer is a type of malignant tumor and the most frequent liver cancer type is hepatocellular carcinoma (HCC) which originates from liver and constitutes about 90% of liver cancer (Fong *et.al.*, 2015). HCC is reported as to be the third leading cause of cancer-related death worldwide (Ferlay *et.al.*, 2010; Jemal *et.al.*, 2011).

1.3 Treatment Strategies for Liver Cancer

Although there are extensive amount of studies focusing on the treatment of liver cancer, it is still one of the most difficult cancer to treat. Treatment strategies for liver cancer usually differ according to stage of the disease. For patients with early liver cancer are surgical resection, partial hepatectomy, adjuvant therapy after surgery, or liver transplantation, and locoregional therapy, while treatment for patients having intermediate HCC involves TAE (embolic particles without chemotherapy) or TACE (chemotherapeutic drugs and embolic particles) therapy to induce tumor necrosis. Patients with advanced HCC are usually treated with systemic therapies such as cytotoxic chemotherapies, immunotherapy, and oncolytic virus therapy. New approaches for treatment are now involving multiple disciplines. Multimodal treatment alternatives are becoming new trends, since they are more specific compared to old fashioned treatments (Liu *et.al.*, 2015).

1.3.1 Chemotherapy for Liver Cancer

Although there is no standard chemotherapy approach to treat hepatocellular carcinoma, there are several agents that are actively used. A multiple kinase inhibitor, Sorafenib, is used as frontline therapy due to its ability to repress the activity of Raf-1 and other tyrosine kinases by inhibiting phosphorylation of MEK/(ERK) cascade (Liu *et.al.*, 2016). Also, another anti-cancer agent, doxorubicin (DOX) is one of the most common drugs used in HCC treatment. DOX is an anthracycline antibiotic that can slow down growth and proliferation of cancer cells by disrupting topoisomerase-II-mediated DNA repair and producing free radicals, thus damaging cellular membranes, DNA and proteins (Gewirtz, 1999). Moreover, anti-cancer drugs such as 5-fluorouracil and cisplatin are also used as chemotherapeutic agents to treat HCC. However, the success rates of all these treatments cannot exceed 10%, which might be due to toxicity or poor response because of chemoresistance (Asghar *et.al.*, 2012). Since individual response to the same drug vary among patients, combination therapy that may reduce side effects is usually preferred (Zhao *et.al.*, 2015). Besides, although dichloroacetate (DCA) had been thought to be one of the causes of liver toxicity and liver cancer (Herren-Freund *et.al.*, 1987; Bull *et.al.*, 1990; DeAngelo *et.al.*, 1991, 1999; Daniel *et.al.*, 1992; Pereira, 1996) until the last decade, there are various reports that show anti-tumor effects of DCA (Neveu *et.al.*, 2016; Su *et.al.*, 2016; Kankotia *et.al.*, 2014; Zhang *et.al.*, 2011; Pathak *et.al.*, 2014).

1.3.1.1 Dichloroacetate as Anti-Cancer Drug

Dichloroacetate (DCA - $C_2H_2Cl_2O_2$) is an anti-cancer agent due to its ability to reverse Warburg effect, which defines the phenomena that cancer cells obtain their bioenergetic needs from glycolysis rather than glucose oxidation in tumors. Although in 1960s DCA had been known to treat congenital lactic acidosis (Stacpoole *et.al.*, 2008) and had effects on hypercholesterolemia (Stacpoole *et.al.*, 1970), recent studies showed its anti-tumoral effect mainly by altering the mitochondrial metabolism (Roche *et.al.*, 2001; Kato *et.al.*, 2007; Pathak *et.al.*, 2014).

DCA is considered as a mitochondrial kinase inhibitor, since it is capable of changing abnormal metabolism of cancer cells from glycolysis to glucose oxidation through its inhibitory effect on pyruvate dehydrogenase kinase 1 (PDK1), thereby causing positive regulation of pyruvate dehydrogenase (PDH) (Stacpoole, 1989). This inhibition stimulates the conversion of pyruvate into Acetyl-CoA, thus the activation of oxidative phosphorylation. It was found that, DCA administration causes a reduction in high mitochondrial membrane potential and an increase in free radicals, especially reactive oxygen species (ROS) generated via the action of mitochondrial enzymes in cancer cells but not in healthy cells (Bonnet *et.al.*, 2007; Pathak *et.al.*, 2014). By this way, DCA promotes apoptosis, reduces high mitochondrial membrane potential in cancer cells and slows down or stops cancer cell proliferation and growth. Despite its potential for mitochondria-targeted cancer treatment, its uptake by mitochondria is considerably low due to its negative charge (Michelakis *et.al.*, 2008). Therefore, the pharmacological dose required to show desired anti-tumor effect is significantly high that may lead to severe side effects, including liver toxicity.

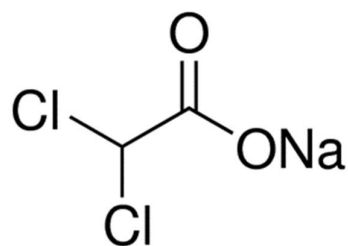


Figure 1.1 Chemical structure of sodium dichloroacetate (Na-DCA)

1.3.1.2 New approach for DCA delivery

Most common way of delivering DCA involves conjugation with sodium salt (Na-DCA) (Kankotia *et.al.*, 2014), but its uptake still cannot reach a desired concentration. New steps that was taken in order to increase the uptake involves the modification DCA with lipophilic phosphonium cations such as triphenylphosphonium (TPP) which is also used because of its ability to utilize the large mitochondrial membrane potential ($\Delta\psi_m$, negative inside) to increase the accumulation (Murphy *et.al.*, 2007; Finichiu *et.al.*, 2012). These cations form a positively charged complex when they are conjugated with DCA, so this allows the complex to cross the mitochondrial inner membrane.

1.4 Nanobiotechnology in cancer and drug delivery

Nanobiotechnology is an important branch of nanotechnology in which different disciplines such as genomics, proteomics, chemistry, physics and engineering are combined. Nowadays, nanobiotechnology has a significant potential in the discovery and development of new tools, biodegradable materials and biomolecular-sensing applications and it provides an ever-growing understanding in the study of life (Malekzad *et.al.*, 2018). The field has a great impact on many industrial applications and new discoveries such as drug delivery systems, tailor-made gene therapy, imaging, artificial organs, and micro-/nanobiomaterials (nanoparticles, nanosized microchips etc.) (Shi *et.al.*, 2010; Ruggiero *et.al.*, 2010), and the aim is to use these developments at the molecular level. Currently, most of the potential therapeutic drugs have poor pharmacokinetic properties, which creates a need for an improvement in drug delivery. Development of new biocompatible nanocarriers such as nanoparticles provides novel ways for targeted drug delivery without damaging and affecting other tissues and organs (Liu *et.al.*, 2007; Singh *et.al.*, 2009).

These nanocarriers also provide a direct targeting to tumor cells by using the properties of cancer cells which is quite different from the healthy ones. For example, it was shown that, the extracellular pH of cancerous tissue is much lower than that of the normal tissue (Ruggiero *et.al.*, 2010). Using this knowledge, biodegradable nanomaterials, which are broken at low pH that corresponds to tumor microenvironment but not at higher pH, could be produced and healthy tissues can be saved. Moreover, another difference between cancer and normal tissues is shown in the glucose uptake rate. New treatment methods now include therapies that blocking glucose uptake by cancer cells with time instead of changing or slowing metabolism of these cells (Kalyanaraman, 2017). Normal cells do not utilize glucose to form lactate in the presence of oxygen. As opposed to healthy cells, cancer cells metabolize glucose to lactate to meet energy requirement for their survival although oxygen is available, a phenomenon termed as Warburg effect as shown in Figure 1.2 (Koppenol *et.al.*, 2011).

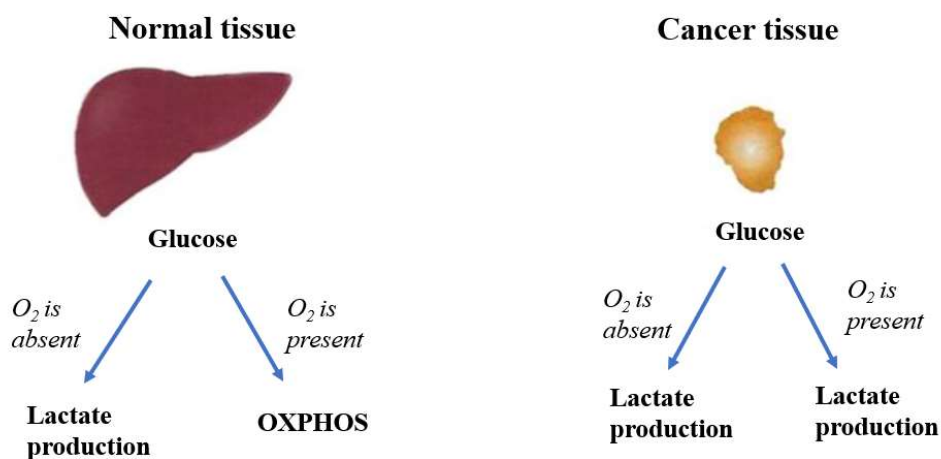


Figure 1.2 Metabolic differences in normal and cancer cells and tissues. OXPHOS refers to oxidative phosphorylation. (Kalyanaraman, 2017).

This metabolic difference is one of the first defined characteristics referred as trademark of cancer cells. Cancer cells are highly glycolytic since they have to metabolize much more glucose to obtain necessary energy for their survival.

Thus, their glucose uptake is considerably higher compared to normal cells and this uptake is facilitated through glucose transporters (GLUTs) that are known to be overexpressed in cancer cells (Kalyanaraman, 2017). According to literature, fluorodeoxyglucose uptake through GLUT1 channels is significantly higher in aggressive Her2-positive mammary tumor (Alvarez *et.al.*, 2014), and GLUT1 protein is known to be overexpressed in highly aggressive cancer cell lines (Chen *et.al.*, 2010; Cao *et.al.*, 2013). Since glycolysis is the only energy-producing process in cancer cells, blocking any step of this pathway by using selectively targeted drugs could be a potential approach to cancer therapy. Thus, cancer cells can be inactivated without damaging other tissues by selectively inhibiting GLUT channels, which was accomplished by the internalization of glucose-coated magnetic nanoparticles (Venturelli *et.al.*, 2016). Also, one of the anticancer strategies focusing inhibition of glycolytic pathway involves 2-deoxyglucose (2-DG), a competitive inhibitor of glucose metabolism that inhibits hexokinase-2 activity which is highly expressed in cancer cells compared to normal cells (Pelicano *et.al.*, 2006; Roberts *et.al.*, 2015). Although using only 2-DG in cancer treatments has not been successful yet, but still it offers a promising approach in multimodal cancer therapy (Muley *et.al.*, 2015; Wang *et.al.*, 2015). Hence, coating nanoparticles with 2-DG not only increases the uptake of NPs through GLUTs, but also it helps blocking cancer growth by inhibiting at the very first step of glycolysis.

1.4.1 Nanoparticles

The reason why nanoparticles (NPs) are attractive for medical purposes is based on their important and unique features, such as their surface to mass ratio that is much larger than that of other particles, their quantum properties and their ability to adsorb and carry other compounds. NPs have a relatively large (functional) surface which is able to bind, adsorb and carry other compounds such as drugs, probes and proteins (Jong *et.al.*, 2008). Among them, polymeric NPs have a significant potential to develop more efficient therapeutic anti-cancer drugs by driving targeted delivery and controlled release of the drugs to the sites of interest. By controlling their thickness and composition and modifying these polymeric NPs with potential therapeutic agents and other ligands that help to induce their uptake by the desired tissues is one of the promising approaches for cancer treatment (Karlsson *et.al.*, 2018). These NPs carrying drugs (nanomedicines) can decrease severe side effects produced by prohibitive doses of anti-cancer drugs by loading them with smaller doses of chemotherapeutic agents that would directly target cancer cells (Schoonen *et.al.*, 2014). There are many different types of inorganic NPs composed of gold (Ekin *et.al.*, 2014; Madhusudhan *et.al.*, 2014; Darfarin *et.al.*, 2018) or iron oxide (Zhu *et.al.*, 2014; Truffi *et.al.*, 2018; Kesavan *et.al.*, 2018) that are available also for imaging and sensing for diagnostic applications (Zhu *et.al.*, 2014; Iv *et.al.*, 2015) as well as drug loading and drug release for therapeutic applications (Lin *et.al.*, 2014; Zhao *et.al.*, 2018; DiStasio *et.al.*, 2018; Jayant *et.al.*, 2018; Kesavan *et.al.*, 2018). For example, gold–silicon oxide (SiO₂/Au) core–shell nanoparticles were shown to be a potential radiotherapy option for breast cancer cell line, MCF-7 (Darfarin *et.al.*, 2018). Glucosaminic acid-modified magnetic nanoparticles (GA-MNP) showed a great solubility in water and they were stable, however, their cellular uptake required over 5-day exposure (Yu *et.al.*, 2008). Also, it was found that, the pullulan super magnetic iron oxide nanoparticle (Pn-SPIONs) exposure decreased cell viability and cell adhesion (Gupta *et.al.*, 2005).

According to Iv and coworkers, ultra-small superparamagnetic iron oxides had an effective role in diagnostic and therapeutic neuro-oncologic setting in brain tumor (Iv *et.al.*, 2015).

In our study, iron oxide nanoparticles are chosen for drug (DCA) delivery for therapeutic purposes.

1.4.1.1 Iron Oxide Nanoparticles

In recent years, the use of smart and biocompatible NPs is becoming new trends in biomedical applications, since they have different properties and can be tailored according to its purpose, avoiding the unwanted side effects (Seabra *et.al.*, 2013; Nazir *et.al.*, 2014). One of the promising nanomaterials drawing attention is the iron oxide nanoparticles, especially magnetite (Fe_3O_4) with a core ranging between 10 nm and 100 nm in diameter (Wahajuddin *et.al.*, 2012). Iron oxide nanoparticles (IONPs) have attracted much consideration due to their unique properties, such as superparamagnetism, surface-to-volume ratio, greater surface area, and easy separation methodology. These NPs are being widely used in various biomedical applications including the diagnostic purposes, targeted drug delivery, and hyperthermia (Haddad *et.al.*, 2012; Chen *et.al.*, 2012; Gajalakshmi *et.al.*, 2013; Cai *et.al.*, 2014).

1.4.1.2 Surface Modifications

Although iron oxide NPs (Fe_3O_4) that are also known as magnetic nanoparticles are considered as promising nanomaterials among others due to their chemical and physical properties, low bioavailability and biocompatibility are one of the most important disadvantages of using these materials.

Despite their common usage by scientific community, their toxicity is another significant drawback (Seabra *et.al*, 2014). Iron oxide magnetic nanoparticles due to having chemical nature different than biological components, do not act in the same way, causing undesired outcomes such as cell membrane adhesion, cell death, or cell growth (Gupta *et.al.*, 2005; Auffan *et.al.*, 2006). In order to be able to use these iron-based magnetic nanoparticles safely in biomedical applications, some surface modifications for a desired purpose should be carried out.

Coating iron-based MNPs with biocompatible materials can increase uptake efficiency, neutralize cytotoxic effects produced by these nanoparticles to only exert the function of conjugated drug of interest since they are nontoxic or relatively less toxic, whereas uncoated iron oxide nanoparticles promote a significant reduction in metabolic activity and cell proliferation in the human body (Jian *et.al.*, 2014; Brunner *et.al.*, 2006). Besides, coating with biodegradable materials can stabilize the nanoparticle systems, decreasing the opsonization risk by phagocytic system along blood circulation in the body (Eidi *et.al.*, 2010; Kemp *et.al.*, 2010). Also, this surface modification provides a framework for conjugation with biological moieties or therapeutic agents for cancer targeted treatment (Bava *et.al.*, 2013; Mora-Huertas *et.al.*, 2010). Among coating materials, heparin, an anticoagulant agent, is widely used due to its ability to mask toxicity of nanoparticles and improve the biocompatibility of nanocarriers (Singh *et.al.*, 2007; Garg *et.al.*, 2017). Heparin coated nanoparticles can be used in various biomedical applications such as tissue engineering, cancer therapy and targeted drug delivery, and diagnostic applications (Kemp *et.al.*, 2010; Bava *et.al.*, 2013).

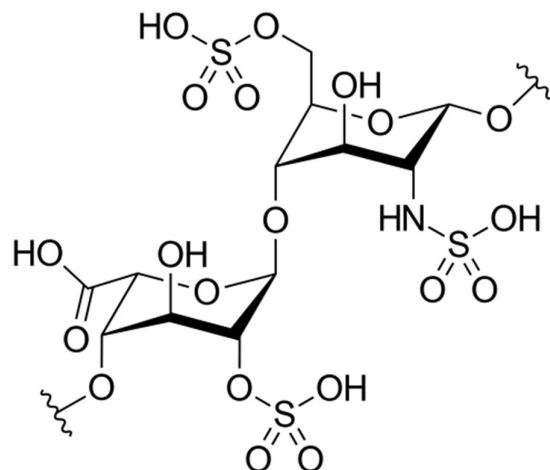


Figure 1.3 Chemical structure of heparin

1.4.1.3 Two-layer Heparin Coated TPP-DCA conjugated 2-D-Glucose Attached Iron Oxide Nanoparticles

Nanoparticles (IONPs) that are used in this study are prepared in Prof.Dr. Mürvet Volkan's laboratory at Department of Chemistry (METU) (Akpınar, 2017). Heparin is used as coating material to improve biocompatibility. As heparin layer increases on surface of the nanoparticles, not only solubility of NPs, but also NP uptake rate by cancer cells were increased. Using the advantage of the negative charge of heparin, dichloroacetate (DCA) conjugated with positively charged triphenylphosphonium (TPP) was embedded in this heparin layer and an additional heparin layer conjugation was performed via ionic interaction. The positive charge on TPP help the internalization of DCA by mitochondrial membrane and this internalization eventually would lead to inhibition of PDH kinase, thereby reversing Warburg effect by stimulating pyruvate to Acetyl-CoA conversion for oxidative phosphorylation, the process cancer cells do not prefer, since they are highly glycolytic.

Furthermore, using the differences in the expression of GLUT channels in cancer cell lines in which glucose uptake is much higher than healthy cells, heparin coated nanoparticles were conjugated with 2-D-Glucose which will help for the internalization of the NPs and eventually inhibiting glycolysis by both blocking hexokinase-2 and further glucose uptake.

1.5 Aim of the Study

The aim of the study is to design a nanoparticle which can be an effective way for DCA transport into hepatocellular carcinoma HepG2 cells. For this reason, we collaborated with Prof.Dr. Mürvet Volkan's laboratory at Chemistry Department and iron oxide nanoparticles (Fe_3O_4) were prepared for DCA delivery into liver cancer cells. In order to improve biocompatibility, the surface of the NPs was modified with heparin.

Further, to increase the rate of internalization of NPs into the cells, 2-D-Glucose was attached so that final product can use GLUT II transporters. The design of nanoparticles was then carried out in the light of the biological experiments which were used to optimize DCA delivery into cells. Then HepG2 cells were treated with these NPs in order to see their cellular uptake and possible cytotoxic effects for successful drug delivery. The effect of the drug was tested by looking at the apoptotic potential and the change in the mitochondrial membrane potential of the cells.

CHAPTER 2

MATERIALS AND METHODS

2.1 Materials

All laboratory equipment used in cell culture and assays performed outside of the cell culture were analytical and cell culture grade. In cell culture experiments, T-25/T-75 cell culture flasks and 6 well/ 96-well cell culture plates, (Sarstedt, Germany or Grenier-Bio, Germany), Cryovials (Grenier-Bio, Germany), micropipettes (Eppendorf, Germany), multichannel Pipette 200 μ L (Rainin, Mettler-Toledo, USA), pipetgun (Isolab, Germany), sterile filtered pipette tips (Grenier-Bio, Germany, Axygen, USA), serological pipettes (Sarstedt, Germany), polypropylene centrifuge tubes (Sarstedt or Isolab, Germany), centrifuge tubes (Sarstedt, Germany) and BrightLine hemacytometer (Marienfeld, Germany) have been purchased from different companies.

All chemicals were either cell culture grade or sterilized. In cell culture experiments DMEM medium with low glucose, with L-Glutamine, Na-pyruvate and 25mM HEPES (Biowest, France), PBS without Mg⁺² and Ca⁺² (Biological Industries, Israel), heat-inactivated fetal bovine serum (FBS) (Biowest, France), Trypsin-EDTA 10X (Biowest, France), Penicillin-Streptomycin solution (Biological Industries, Israel), dimethyl sulfoxide (DMSO) (Applichem, Germany), and 5% Trypan blue solution (Biological Industries, Israel), formaldehyde solution 37%, stabilized (Sigma-Aldrich, USA) were used.

In cytotoxicity and flow cytometry experiments, commercially available Cell Proliferation kit XTT Based (Biological Industries, Israel), Flow Cytometer Fluid Kit (BD Biosciences, USA), Annexin V-FITC Apoptosis Detection Kit (Abcam, UK), and Mitochondria Membrane Potential Kit (JC-10 assay) (Sigma-Aldrich, USA) were used.

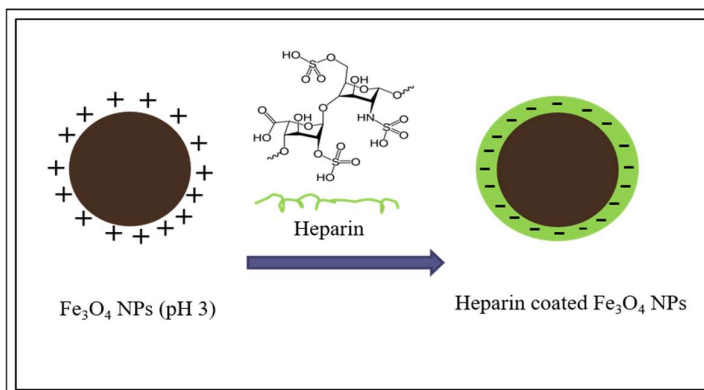
HepG2 cell line is a hepatocellular carcinoma cell line which was obtained from a 15 year-old Caucasian male purchased from ATCC (American Type Culture Collection).

2.2 Methods

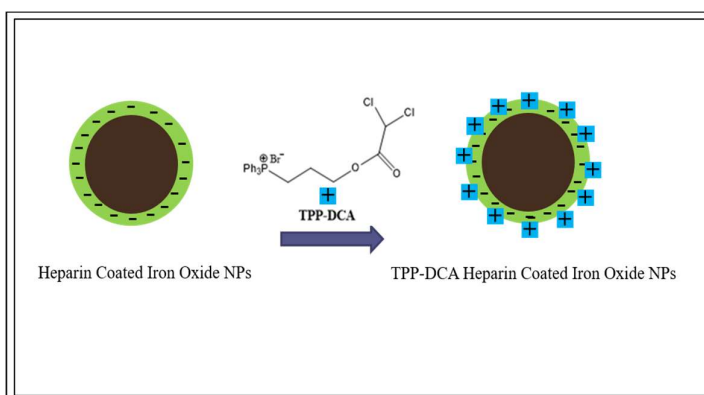
2.2.1 Preparation of Nanoparticles

Nanoparticles (NPs) used in this study were prepared at Department of Chemistry (METU) under the supervision of Prof.Dr. Mürvet Volkan (Akpınar, 2017). Iron oxide nanoparticles (IONP), Fe_3O_4 , were synthesized by coprecipitation method (Lin *et al.*, 2010) and covered with a heparin layer through ionic interaction. Using the advantage of the negative charge of heparin, TPP-DCA which was positively charged was embedded in this heparin layer and an additional layer conjugation was performed via an ionic interaction. Finally, NPs were conjugated with 2-Deoxy-D-Glucose by EDC/NHS coupling reaction (Xiong *et al.*, 2012).

A.



B.



C.

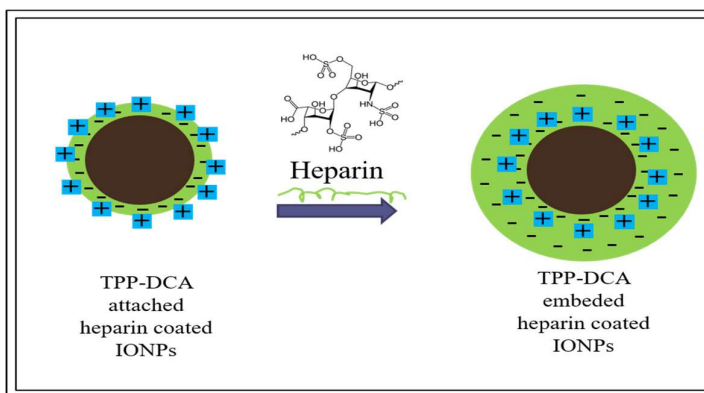


Figure 2.1 Preparation of heparin coated iron oxide nanoparticles conjugated with TPP-DCA. A) Heparin coating, B) TPP-DCA conjugation, C) Additional heparin coating (Akpinar, 2017).

2.2.2 Cell Culture

2.2.2.1 Cell Culture Conditions and Medium

Human hepatocellular carcinoma cell line, HepG2, was grown in Dulbecco's Modified Eagle's medium (DMEM) low glucose with L-Glutamine, sodium pyruvate, and 25 mM HEPES (Cat.No: L0065, Biowest) which was supplemented with 10% fetal bovine serum (FBS) and 1% Pen-Strep solution that were kept at -20°C freezer (Uğur, Turkey) for long time storage, +4°C refrigerator (Arçelik, Turkey) for short term storage. Old medium was changed with fresh one every 2 days and cells were maintained at 37°C atmosphere with 5% CO₂ incubator with water jacket (Series 8000 WJ Thermo-Scientific, USA). All cell culture experiments were performed in Laminar flow cabinet (MN 090, NUVE, Turkey).

2.2.2.2 Treatments

Nanoparticles were first washed with complete medium twice in order to get rid of undesired contaminants. During the washing process, paramagnetic NPs were suspended in 5 mL of complete medium in falcon tubes and kept near a strong magnet to pull all the NPs towards the magnet whereas other contaminants in the falcon tubes were discarded. After washing, nanoparticles were suspended in complete medium containing 0.1% DMSO and dilutions (50-750 µg/mL) were carried out for further experiments. For each experiment, fresh NP stocks were prepared.

2.2.2.3 Cell Seeding

Cryofrosted cells were first kept in a water bath (WiseBath Water Bath, Wisd Laboratory Instruments-Verkon, Czech Republic) at 37°C for 1-2 minutes until they were semi-melted. Then dissolved cells were mixed with 5-6 mL of complete medium in a 15 mL falcon tube, and cells were centrifuged at 1000 rpm for 5 minutes at room temperature (Eppendorf Centrifuge 5810 R, Eppendorf, Germany) to get rid of DMSO present in freezing medium. Supernatant was removed and pellet containing cells were dissolved in 10 mL of complete medium. Then cells were seeded into a T-75 flask and were placed into the CO₂ incubator at 37°C and 5% CO₂ conditions.

2.2.2.4 Cell Growth and Passaging

After one-day incubation following cell seeding, old medium was discarded and cells were washed with 5 mL of PBS before 10 mL of pre-warmed fresh complete medium was added into the flask and were placed at CO₂ incubator for further incubation until cells reached to sufficient confluency that is around 80%.

When cells reached an 80-85% confluency, medium was removed and cells were washed with 5 mL of PBS without Mg⁺² and Ca⁺². After washing step, 2 mL of 1X Trypsin/EDTA solution was added into the flask for cell detachment and were incubated at 37°C and 5% CO₂ for 3-5 minutes. Following incubation, 6 mL of fresh complete medium was added into the flask to neutralize the effect of trypsin and mixed well by pipetting gently. Final volume of 8 mL cell suspension was separated into two new flasks. Then the volume in the flasks was completed to 10 mL by adding 6 mL of fresh complete medium and the cell suspensions in each flask were mixed with pipetting. After this passaging process, cells were replaced into the incubator and maintained at 37°C and 5% CO₂ for further incubation.

2.2.2.5 Cell Freezing

Cells were harvested according to the procedure given previously in section 2.2.2.4. Eight milliliters of cell suspension (2 mL trypsin + 6 mL complete medium) in the flask was mixed well by pipetting and was transferred into a 15 mL falcon tube and further centrifuged at 1000 rpm for 5 minutes. Later, supernatant was discarded, remaining pellet was resuspended in 1 mL of freshly prepared cold freezing medium containing 90% FBS and 10% DMSO and this suspension was transferred into a cryovial immediately. Cryovials were first placed into Mr. Frosty™ Freezing Container (Sigma-Aldrich, USA) and placed into a -80°C freezer (Sanyo -86°C ULT Freezer, Japan) for one day. Later, all cryovials were transferred into a liquid nitrogen tank for long term storage.

2.2.2.6 Cell Counting

Viable cells were counted with a hemocytometer by staining the cell suspension with Trypan Blue. After harvesting the HepG2 cells, pellet obtained from centrifugation step was resuspended in medium and 1 volume (50 µL) of cell suspension solution was mixed well with 1 volume (50 µL) of 0.25% Trypan Blue Solution to analyze cell viability. Then, 10 µL of this final cell suspension containing trypan blue-treated cells were applied onto the chambers of the hemocytometer which was covered with a coverslip allowing the suspension to diffuse through capillary action. Viable cells were easily distinguished under a light microscope (BH-2 Research Microscope, Olympus, Japan) with a 10X objective since trypan blue cannot penetrate into alive cells through their cell membranes, whereas dead cells establish blue color due to staining as shown in Figure 2.2.

Each chamber of the hemacytometer was with the volume of 0.0001 mm^3 , thus the calculations were done by taking average cell count of the chambers and multiplying with 10^4 . The formula is given below;

$$\text{Total Cell Number/mL} = (\text{Average Cell Count of Two Chambers} \times \text{DF} \times 10^4)$$

DF = Dilution Factor

10^4 = Factor that is calculated from the dimension of hemacytometer

Equation 2.1 Formula of total cell count

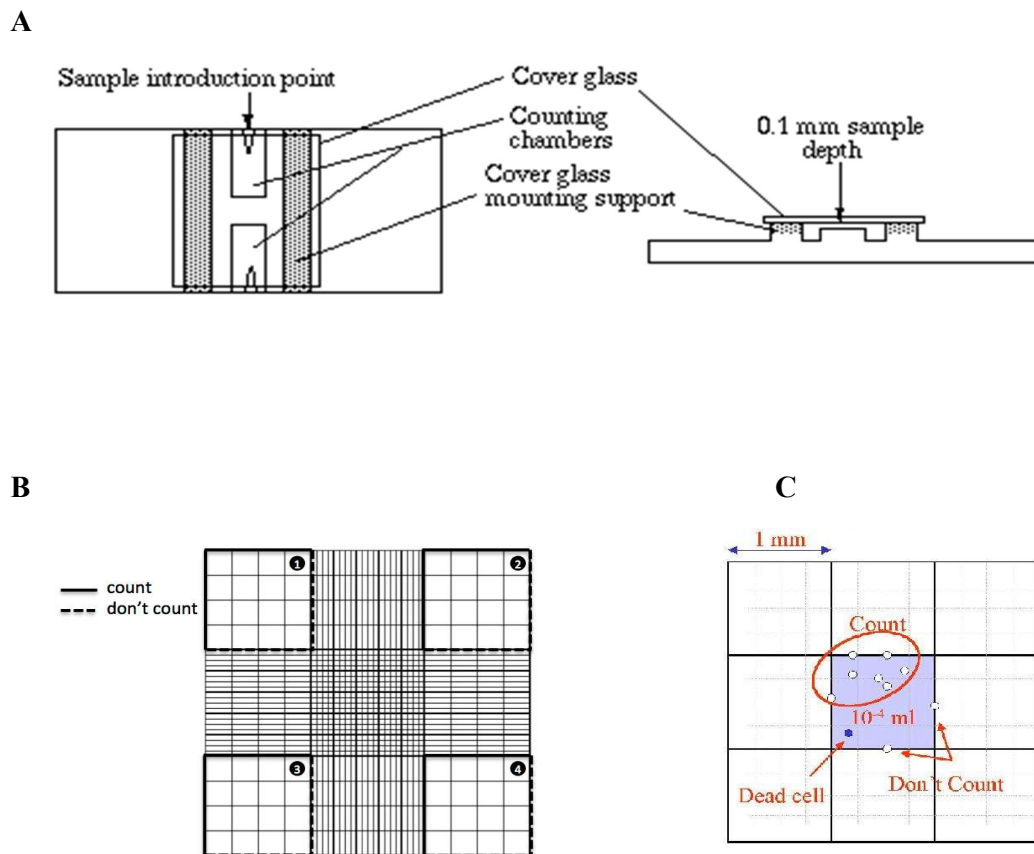


Figure 2.2 (A) Hemacytometer chamber, (B,C) Counting technique.

2.2.3 Cytotoxicity Assays

2.2.3.1 XTT Cell Proliferation Assay

2,3-Bis-(2-Methoxy-4-Nitro-5-Sulfophenyl)-2H-Tetrazolium-5-Carboxanilide (XTT) cell proliferation kit was used to evaluate cytotoxicity of NPs on HepG2 cells according to the manufacturer's instructions with slight modifications. The logic behind this assay relies on the metabolism of the yellow tetrazolium salt XTT that is reduced to orange colored formazan compounds which are water-soluble by the activity of mitochondrial dehydrogenase enzymes of the metabolically active cells (Koban *et.al.*, 2012) as shown in Figure 2.3. The water-solubility of this formazan products allow them to be observed and quantified by using an ELISA reader (Multiskan™ GO- Thermo Scientific, USA).

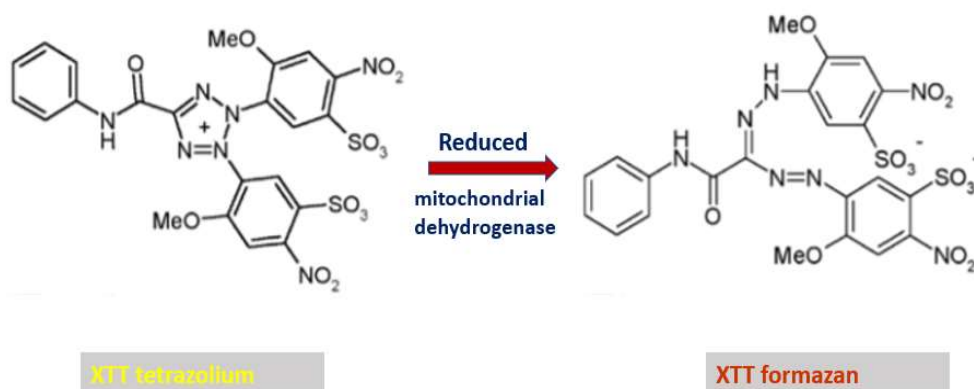


Figure 2.3 Formation of XTT tetrazolium to XTT formazan product

Cells which were grown in T-75 flasks until 80% confluency were harvested and a cell suspension at a concentration of 100,000 cells/mL was prepared. The cells were then transferred onto 96 well plates as 10,000 cells per well (100 μ L/well) for XTT assay and kept 24 hr for cells to attach.

After incubation, medium was discarded from wells and cells were washed with 50 μ L PBS and 100 μ L of medium containing serial dilutions of NPs (50-750 μ g/mL) were added onto the wells. After a 24 hour of incubation, as additional steps to the manufacturer's procedure, a magnet was kept at the top of the 96-well plate for 30 seconds in order to remove NPs that reside in the medium as they failed to enter into the cells (magnetic wash) by taking advantage of their paramagnetic ability of the NPs. Then the medium in the wells containing remaining NPs were discarded and wells were washed with 50 μ l of PBS twice in order to get rid of all black-colored NPs, except the ones which had entered into the cells, since they interfere with the absorbance readings of XTT reagent. Immediately after, 100 μ l of fresh growth medium was added onto each well to avoid drying out the cells. Afterwards, frozen XTT compound was melted in a water bath warmed to 37°C until a clear solution was obtained. *Immediately prior to use*, 5 mL of XTT reagent was mixed with 0.1 ml of activation solution for one 96-well plate and 50 μ L of reaction solution was added onto each well containing treated cells and blank wells and the plate was incubated for further 6 hours in an incubator adjusted to 37°C, 5% CO₂ which was a dark environment required for the assay. After 6 hr incubation, absorbance values of each well were measured at 450 nm which is the wavelength that gives maximum absorbance for the formed product, with a reference wavelength at 630 nm which was used to measure non-specific readings by the microplate reader. Later, readings at 630 nm were subtracted from the readings obtained at 450 nm to eliminate non-specific readings. Cell viability percentages were calculated by subtracting absorbance values of blanks wells without cells from that of wells containing cells and dividing results with that of control wells. The formula of cell viability percentages is given below:

$$\% \text{Cell Viability} = \frac{\text{Avg. OD}_{415} \text{ of treated well (with cell)} - \text{Avg. OD}_{415} \text{ of treated well (without cell)}}{\text{Avg. OD}_{415} \text{ of control well (with cell)} - \text{Avg. OD}_{415} \text{ of control well (without cell)}} \times 100$$

Equation 2.2 The formula for % Cell Viability.

Triplicates for wells containing cells and duplicates for blank wells without cells were prepared for each condition as shown in Figure 2.4. The percentage of cell viability in the control group was considered as 100%. The concentration that is required to inhibit 50% of cell growth which is also known as inhibitory concentration to kill 50% of the population, IC_{50} , was determined from cytotoxicity curves.

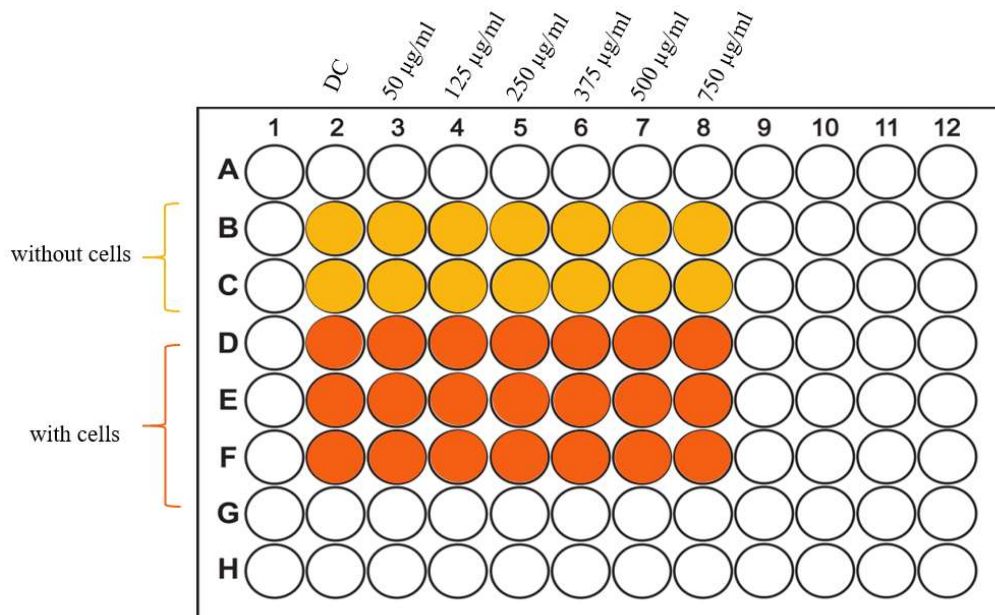


Figure 2.4 Representative template of 96-well plate showing the treatment pattern.
DC: DMSO Control

2.2.3.2 Trypan Blue Exclusion Method

Two hundred and fifty thousand cells were seeded per well in 6 well plates and incubated in a CO_2 incubator at $37^\circ C$ for 24 hours. After incubation, the medium in the wells was discarded and the cells were washed with 1 ml of PBS. Then, the cells were treated with serial dilutions of 2-DG-HEP-TPP-DCA-HEP coated IONPs for 24 hours at $37^\circ C$, 5% CO_2 .

At the end of 24 hr, the medium was removed and cells were washed well with PBS. 0.5 ml of 1X Trypsin/EDTA was added onto each well for cell detachment and the plate was incubated for 3-5 minutes to allow the enzyme to act on cells. Following incubation, activity of trypsin was neutralized by adding 1 mL of fresh complete medium and cells in the wells were collected into Eppendorf tubes. As given in section 2.2.1.6, 1 volume of cell suspension (50 μ L) and 1 volume of 0.25% trypan blue (50 μ L) were mixed well by pipetting and percentages of cell viability for each condition were calculated according to the control wells in which cell viability considered as 100%.

2.2.4 Visualization of Cells Treated with Nanoparticles

Cells treated with NPs as given in section 2.2.3.2 were visualized by taking images under Olympus CKX41 Inverted Microscope (Olympus, Japan) with camera attachment (Olympus, Japan). Images were taken for the following conditions:

- before and after 24 hr treatment with 2-DG-HEP-TPP-DCA-HEP coated IONPs,
- immediately after treatment and after 24 hr treatment with 2-DG-HEP-TPP-DCA-HEP coated IONPs,
- with and without magnetic wash of 24 hr-treated cells with 2-DG-HEP-TPP-DCA-HEP coated IONPs,
- after 24 hr treatment with different NPs during the optimization studies (Naked NPs, 2-DG-TPP-DCA-HEP coated IONPs (*1-layer Heparin with 2-D-Glucose*), 2-DG-HEP-TPP-DCA-HEP coated IONPs (*2-layer with 2-D-Glucose*) HEP-TPP-DCA-HEP coated IONPs (*2-layer Heparin without 2-D-Glucose*)).

2.2.5 Determination of Cellular Uptake of Nanoparticles

Cellular uptake of NPs was determined by using flow cytometry (BD C6+ Accuri Flow Cytometer, BD BioSciences, USA) according to the method developed by Suzuki et al. (Suzuki *et.al.*, 2007).

The principle of this assay is based on the differences in the intensity of the scattered light in flow cytometry. The forward scattered (FSC) light represents cell size while side-scattered (SSC) light represents complexity/granularity of the cell. Thus, while FSC light remain constant during uptake of non-fluorescent nanoparticles, SSC light increases as the concentration of nanoparticles increase inside of the cells as represented in Figure 2.5.

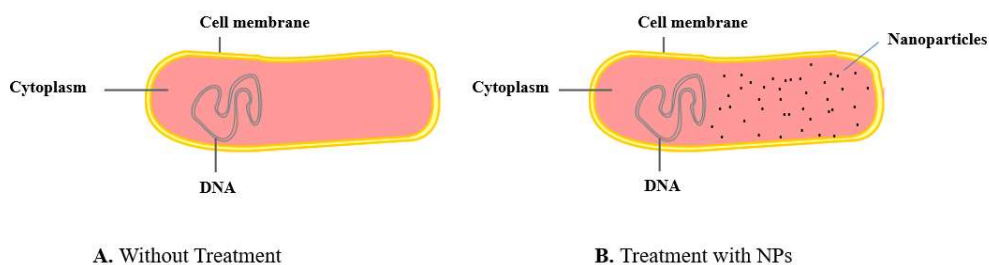


Figure 2.5 Representation of increase in cell granularity in response to cellular uptake of the cell. While cell size remains constant, granularity/complexity of the cell increases with the exposure of NPs.

For the assay, 10^5 cells/well were seeded in 6-well plates. After 24 hr for cell attachment, cells were treated with varying concentrations of different NPs (Naked, 1-layer Heparin with 2-D-Glucose, 2-layer Heparin with 2-D-Glucose, 2-layer Heparin without 2-D-Glucose) for further 24 hours. The medium containing excess NPs were removed and cells were washed at least three times with PBS. Then, cells which were harvested according to the section 2.2.3.2., were collected into Eppendorf tubes and centrifuged at 1000 rpm for 5 minutes, and supernatant was discarded. Remaining pellet was washed to get rid of excess NPs failed to enter into the cells by re-suspending in 1 ml of PBS and, re-centrifuged at 1000 rpm for 5 minutes and supernatant was again discarded. Tubes containing cell pellets were put onto ice, and 500 μ L of 4% formaldehyde was added dropwise carefully while cells were vortexed very slowly (LP Vortex Mixer, Thermo Scientific, USA).

After cells were incubated for about 15 minutes at 4 °C fridge, they were centrifuged at 1000 rpm at 4 °C for 5 minutes and supernatant was discarded. Remaining pellet was resuspended in 1 mL of cold PBS and the cellular uptake of NPs was determined by flow cytometer equipped with a 488 nm laser using FSC vs SSC channels.

2.2.6 Annexin V-FITC Apoptosis Assay

Annexin V-FITC Apoptosis Detection Kit (Abcam) was used to investigate the apoptotic effects of 2-DG-HEP-TPP-DCA-HEP coated IONPs on HepG2 cell line according to the procedure described by the manufacturer. The principal of the assay is based on the disposition of phosphatidylserine (PS) found on the lipid membrane during apoptotic process. PS resides inner face of the plasma membrane in healthy cells (Fadok *et.al*, 1992; van Engeland *et.al.*, 1998). After initiation of apoptosis, cells translocate their PS to the cell surface which then binds its ligand, Annexin V, that is conjugated with a green fluorescent dye, FITC in this kit. Also, Propidium Iodide (PI) that is offered by the kit stains dead cells by penetrating into the cell through disrupted plasma membrane.

Three hundred thousand cells/well were seeded and grown in a 6-well cell culture plate. They were treated with varying concentrations of 2-DG-HEP-TPP-DCA-HEP coated IONPs for 24 hours and harvested according to the procedure given in section 2.2.4. Cells collected into Eppendorf tubes were centrifuged at 1000 rpm for 5 minutes. After the removal of the supernatant, cells were re-suspended in 500 μ L Binding Buffer containing loads of Ca⁺² ions instead of PBS without Ca⁺², since binding of PS with Annexin V is Ca⁺² dependent. Then, 5 μ L of Annexin V-FITC and 5 μ L of PI offered by the kit were added onto the tubes and cells were incubated at room temperature for 5 minutes followed by the incubation on ice to avoid quenching of the dyes. Annexin V-FITC binding which implies initiation of apoptotic process was analyzed by flow cytometry using FL-1 vs. FL-2 channels.

2.2.7 JC-10 Mitochondrial Membrane Potential Assay

Mitochondrial Membrane Potential Kit, JC-10 based (Sigma-Aldrich) was used in order to investigate the change of mitochondrial membrane potential in response to NP treatment according to the procedure given by the manufacturer. The principle of this assay is based on a mechanism similar to JC-1 that JC-10 which selectively enters into the mitochondria and changes its color, which was observed as green in the cytosol to orange in response to accumulation in mitochondria as the membrane potential increases (Perry et.al., 2011; Chen et.al.2014). In healthy cells, JC-10 is observed as a monomer in the cytosol that is observed as green, and also exists as aggregates in the mitochondria that is stained red. On the other hand, in dead cells or in the cells undergoing apoptosis, only monomeric form of JC-10 (green) can be observed.

Three hundred thousand cells/well were seeded and grown in a 6-well cell culture plate. They were treated with 2-DG-HEP-TPP-DCA-HEP coated IONPs for 24 hours and harvested according to the procedure given in the section 2.2.5. Cells treated with 8.7 μ M of Carbonyl cyanide 3-chlorophenylhydrazone (CCCP) was used as positive control. Cells collected into Eppendorf tubes were centrifuged at 1000 rpm for 5 minutes. After supernatant was discarded, pellet was washed with complete medium once. Cells, then, were re-suspended in 500 μ L of JC-10 Dye Loading solution (10 μ L 200X JC-10 was mixed with 5 mL of Assay Buffer offered by the kit) that was prepared right before the experiment according to the procedure given by the manufacturer with slight modifications since the assay resulted in very strong signals. Cells were incubated at room temperature at dark for 30 minutes. For the negative control, DMSO (DC) incubation time was decreased to 20 minutes, as healthy cells showed a very strong signal that flow cytometry could not read and population was recorded as out of range.

Later, cells were centrifuged at 1000 rpm for 5 minutes and after the supernatant was removed, they were resuspended in 1 mL of Assay Buffer offered by the kit. Then, mitochondrial membrane potential was analyzed by flow cytometry by using FL-1 and FL-2 channels.

CHAPTER 3

RESULTS AND DISCUSSION

3.1 Preparation and Optimization of Nanoparticles

Iron oxide nanoparticles, referred as naked nanoparticles in this study, were prepared by using co precipitation method (Lin, 2011) in Prof.Dr.Mürvet Volkan's laboratory (Akpınar, 2017). Transmission Electron Microscopy (TEM) and X-Ray Diffraction (XRD) measurements were used for the characterization of the nanoparticles (Figure 3.1A) and further optimization studies were carried out in our laboratory.

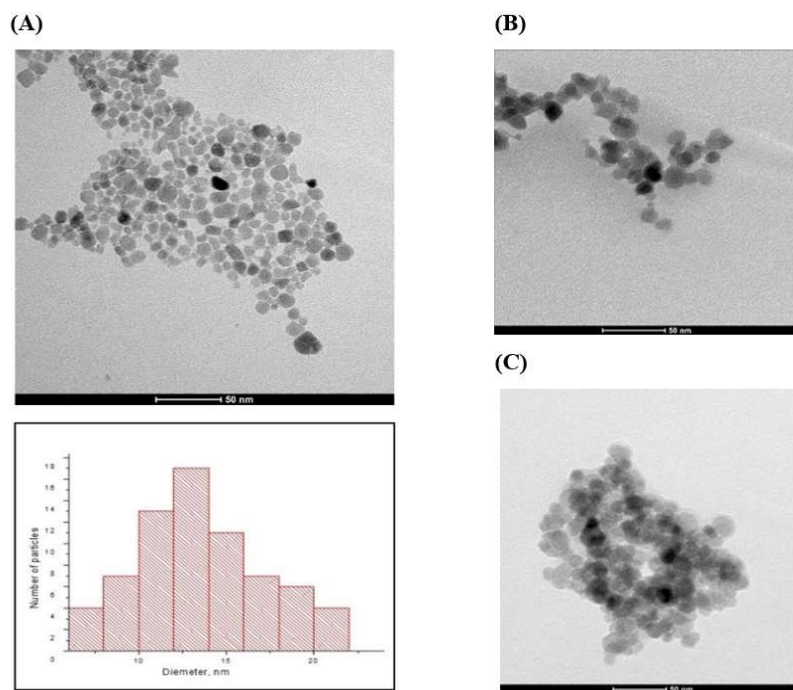


Figure 3.1 TEM image and size distribution of A) Iron oxide nanoparticles (Naked nanoparticles), B) heparin coated iron oxide nanoparticles, C) 2-DG-HEP-TPP-DCA-HEP coated IONPs or 2-L-H TPP-DCA 2-DG NPs.

According to the results obtained from XTT cell viability assay, Trypan blue exclusion method, and cellular uptake assay, iron oxide nanoparticles were first coated with a heparin layer via ionic interaction between negatively charged heparin molecules and positively charged surface of iron oxide nanoparticles and these nanoparticles were referred as heparin-coated nanoparticles having one or two layers (Figure 3.1B). After coating the nanoparticles with one layer of heparin, 110 $\mu\text{g}/\text{mL}$ of TPP-DCA per 1 mg/mL of Fe_3O_4 was embedded into this heparin coated nanoparticles (1-L-H NPs) via ionic interaction and nanoparticles were further covered with an additional layer of heparin (2-L-H NPs) in order to increase the solubility of the nanoparticles and to prevent the potential agglomeration due to magnetic nature of iron oxide nanoparticles. 2-D-Glucose (2-DG) was then attached to the surface of the outer heparin layer for targeting purposes and concentration of 2-DG was calculated as 4.86×10^{-6} M per 1 mg/mL of Fe_3O_4 (Figure 3.1C).

3.2 Cell Culture

3.2.1 Cytotoxicity Assays

3.2.1.1 XTT Cell Proliferation Assay

The intake and cytotoxicity of nanoparticles in HepG2 cells were determined by colorimetric XTT-based cell proliferation assay. In this assay, cells in 96-well plates were treated with various concentrations (50-750 $\mu\text{g}/\text{mL}$) of differently prepared nanoparticles for 24 hours. After 24hr incubation, plates were measured at 450 and 630 nm by an ELISA plate reader and readings at 630 nm were subtracted from readings at 450 nm to eliminate non-specific readings.

The viability of cells was represented by cell viability percentages as means \pm SEM. Cell viability of negative control was shown as 100% and effects of all concentrations were determined with respect to negative control. All calculations were done by using GraphPad Prism 7.04.

XTT assay was performed for differently prepared nanoparticles at various concentrations to observe the effects of molecules used in the preparation of nanoparticles for optimization. At first, the cytotoxicity of only DCA conjugated with sodium salt (Na-DCA) and TPP conjugated with DCA (TPP-DCA) was determined and the results obtained was as expected according to the literature (Pathak, 2014). Even the highest concentration of Na-DCA (in 1000 $\mu\text{g/mL}$ of Fe_3O_4) did not show any significant effect on cell viability (Figure 3.2) since its cellular uptake is considerably low as mentioned in the literature. Although the result was not statistically significant ($p > 0.05$) when these two groups were compared, TPP- DCA showed a slight decrease in cell viability compared to Na-DCA.

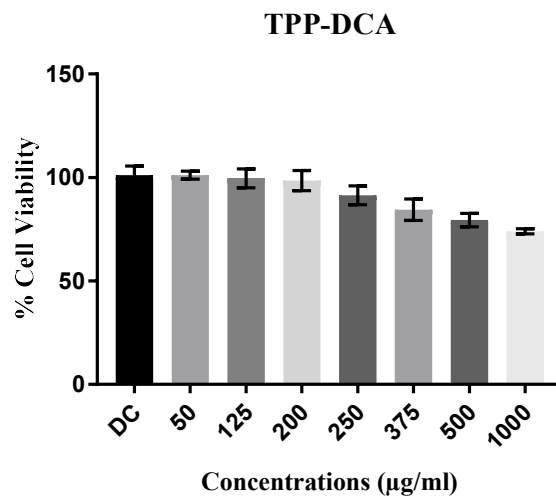
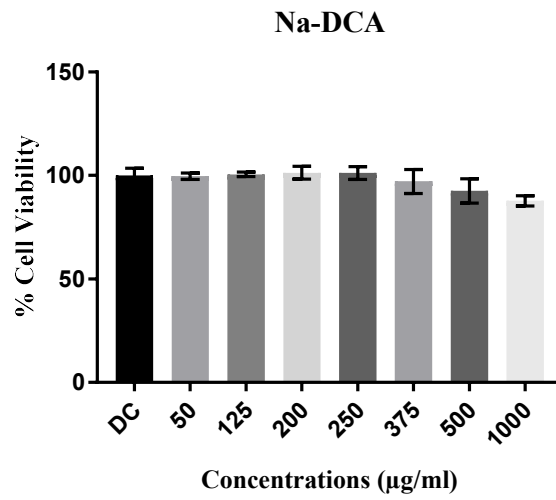


Figure 3.2 The effects of Na-DCA and TPP-DCA on HepG2 cell growth by using XTT assay. The viability of cells was represented as cell viability percentages, means \pm SEM.

Further optimization of nanoparticles by using cell viability was performed for:

- A) naked nanoparticles (Fe_3O_4 only),
- B) one-layer heparin coated nanoparticles with TPP-DCA with 2-D-Glucose (2-DG-TPP-DCA-HEP coated IONPs, or simply 1-L-H TPP-DCA 2-DG NPs),
- C) two-layer heparin coated nanoparticles with TPP-DCA with 2-D-Glucose (2-DG-HEP-TPP-DCA-HEP coated IONPs, or simply 2-L-H TPP-DCA 2-DG NPs)
- D) two-layer heparin coated nanoparticles without TPP-DCA with 2-D-Glucose (2-DG-HEP-HEP coated IONPs, or simply 2-L-H 2-DG NPs)

Preliminary results obtained from XTT Assay (Figure 3.3) were not as expected since the color of the nanoparticles were black and the assay was colorimetric, they most probably interfered with the readings taken by ELISA plate reader. Also, as treatment time increased, nanoparticles aggregated because of their magnetic nature. Therefore, as additional steps to the procedure, we first placed a magnet onto the lid of the plates for 30 seconds, which we called magnetic wash and washed the wells with 50 μl of PBS twice. Then, we add 100 μl of complete medium right before 50 μl XTT reaction mixture and procedure were performed according to manufacturer's instructions.

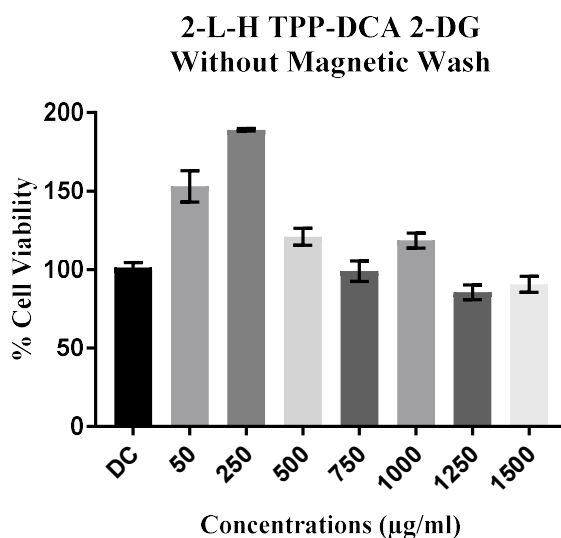


Figure 3.3 XTT Assay results without magnetic wash

According to the results, the effect of naked nanoparticles on cell viability by itself was lower ($p > 0.05$) compared to other coated nanoparticle groups (Figure 3.4, 3.5, and 3.6). Extra heparin layer caused more reduction in cell viability compared to one-layer heparin coating. Moreover, when the results of group C and D were compared (Fig. 3.5 and Fig.3.6), it was seen that the effect of drug of interest, TPP-DCA, on the reduction of cell viability was statistically significant which might indicate that the engineered nanoparticle successfully delivered the TPP-DCA.

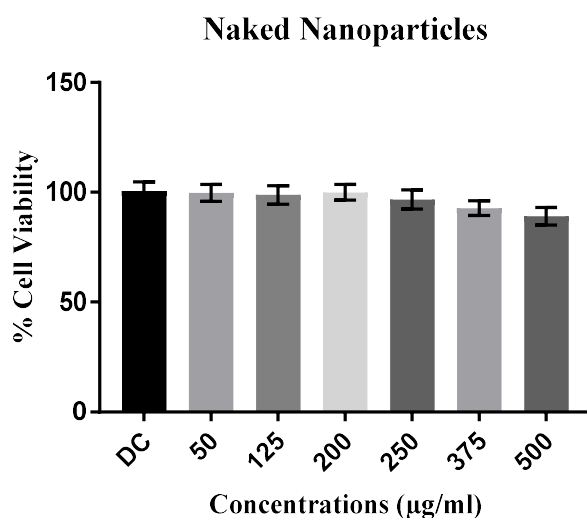


Figure 3.4 XTT Assay results of naked nanoparticles. The viability of cells was represented by cell viability percentages as means \pm SEM. ($p > 0.05$)

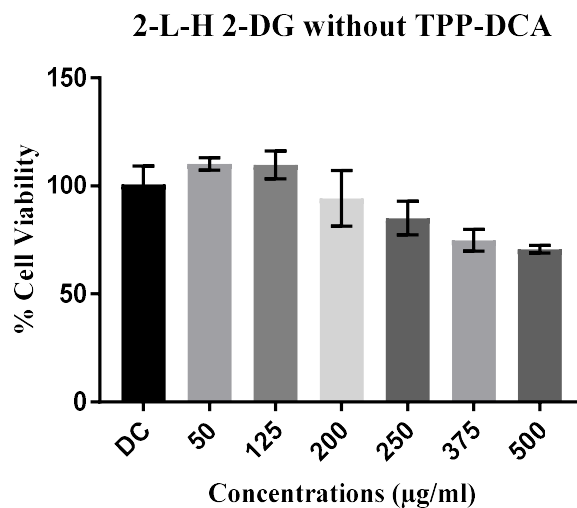


Figure 3.5 XTT Assay results of cells treated with various concentrations of two-layer heparin coated, 2-D Glucose conjugated iron oxide nanoparticles without TPP-DCA for 24 hours. The viability of cells was represented by cell viability percentages as means \pm SEM. ($p > 0.05$)

After these optimization studies, we decided to use 2-D-Glucose attached two-layer heparin coated TPP-DCA conjugated iron oxide nanoparticles (2-DG-HEP-TPP-DCA-HEP coated IONPs, or 2-L-H TPP-DCA 2-DG NPs).

According to XTT results, cell viability percentages of HepG2 cell line were reduced after 24-hour nanoparticle treatment in a dose-dependent manner compared to our DMSO control ($p < 0.001$), since nanoparticle dilutions were prepared in complete medium containing 0.1% DMSO (Figure 3.6). IC₅₀ value was calculated as 525 µg/mL by using Equation 2 and different inhibitory concentrations were given in Table 3.1.

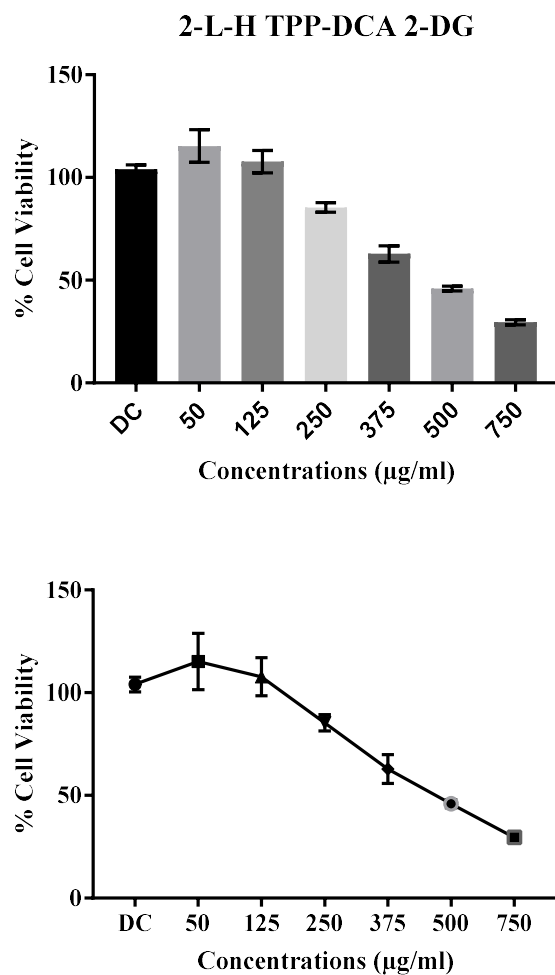


Figure 3.6 Inhibitory effects of 2-L-H TPP-DCA 2-DG NPs on HepG2 cell growth calculated by using XTT Assay. The viability of cells was represented by cell viability percentages as means \pm SEM. ($p < 0.001$)

Inhibitory concentrations of 2-L-H TPP-DCA 2-DG NPs for 24hr treatment		
IC25 (µg/mL)	IC50 (µg/mL)	IC75 (µg/mL)
285	525	750

Table 3.1. Inhibitory concentrations of 2-L-H TPP-DCA 2-DG NPs on HepG2 cell growth.

According to the literature, IC₅₀ values for Na-DCA were determined as 41±9 mM, and 51±17 mM for DU145, and LNCaP cells, respectively, whereas these values for TPP-DCA were as 468±49 µM, and 302±37 µM (Pathak, 2014), thus, IC₅₀ value of Na-DCA alone was 87-fold and 168-fold higher respectively than TPP-DCA. Similarly, according to our results Na-DCA showed almost no effect on HepG2 cells even at high concentrations. IC₅₀ value of 2-D-Glucose attached two-layer heparin coated TPP-DCA conjugated nanoparticles for HepG2 cell line was calculated as 525 µg/mL which contained 55 µg/mL TPP-DCA corresponding to 127.6 µM. Conjugation of TPP-DCA to the prepared nanoparticle was observed to be more effective to inhibit HepG2 cell growth than TPP-DCA alone.

3.2.1.2 Trypan Blue Exclusion Method

The effects of the intake of nanoparticles were also studied by trypan blue exclusion method in parallel to XTT cell viability assay. In this assay, cells in 6-well plates were treated with nanoparticles at concentrations of 250 and 500 µg/mL for 24 hours. After the incubation, cells were subjected to magnetic washing for 30 seconds as in the XTT assay and they were counted. Cell viability of negative control is given as 100% and the effects of all concentrations are determined with respect to negative control.

According to our results, 2-DG attached two-layer heparin coated TPP-DCA conjugated iron oxide nanoparticles were found to be the most effective NPs in terms of inhibiting the cell proliferation, while neither Na-DCA nor naked nanoparticles showed no significant effects as expected (Figure 3.7). Though this method by itself is not reliable enough due to low accuracy, in order to validate the XTT results cell counts were used and the results seem to be well correlated with XTT results.

Furthermore, in order to see whether TPP-DCA is really effective in reducing the cell viability, we treated the cells with two-layer heparin coated nanoparticles with or without TPP-DCA between the concentrations of 250-1000 µg/mL (Figure 3.8).

As seen from the Figure nanoparticles containing TPP-DCA caused more reduction in cell number compared to the ones without TPP-DCA.

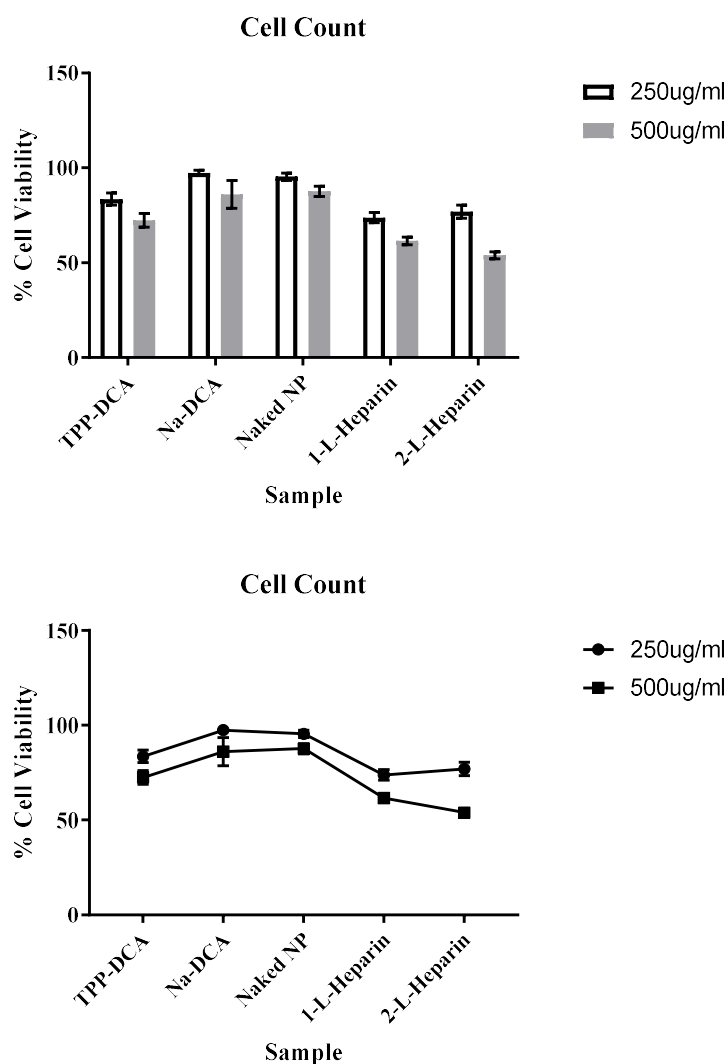


Figure 3.7 Cell counts after 24hr treatment with 5 different samples at concentrations of 250 and 500 µg/mL. 1-L-Heparin refers to 1-layer heparin coated TPP-DCA conjugated 2-DG attached NPs, while 2-L-Heparin represents 2-layer heparin coated TPP-DCA conjugated 2-DG attached NPs.

NPs with TPP-DCA vs NPs without TPP-DCA

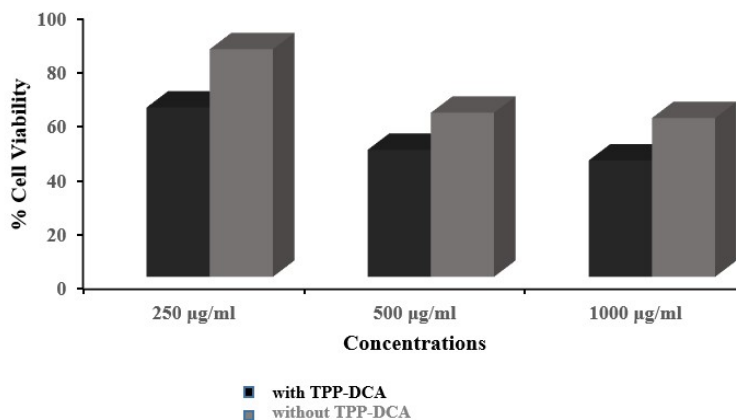


Figure 3.8 Comparison of cell viability treated with two-layer heparin coated nanoparticles with or without TPP-DCA at three different concentrations namely 250, 500, and 1000 µg/mL.

3.2.2 Visualization of Cells by Light Microscopy

Cells treated with nanoparticles were visualized under Olympus CKX41 Inverted microscope using attached camera (Figure 3.9). As seen in Figure 3.9, addition of an extra heparin layer increased the solubility of the nanoparticles. In cells treated with one-layer heparin NPs, nanoparticles were seemed to be more aggregated compared to two-layer heparin NPs. Also, in Figure 3.10 microscope images showed that, NPs without heparin coating were more likely to agglomerate than heparin coated NPs. The effect of magnetic wash is given in Figure 3.11. As nanoparticles are black-colored and they tend to aggregate, as the treatment time increased, they formed black-colored complexes even bigger than the cell itself and they stick to the surface of wells which makes the removal of excessive materials quite hard. Thus, in addition to PBS washing, we also performed a magnetic wash step by using the magnetic properties of the nanoparticles which helped to get rid of the waste materials.

Presence of excess NPs which formed black-colored aggregates interfered with colorimetric XTT assay also, in which an increase in red color intensity was observed. Therefore, with this extra magnetic wash step, we also eliminated any misleading results coming from the color interference.

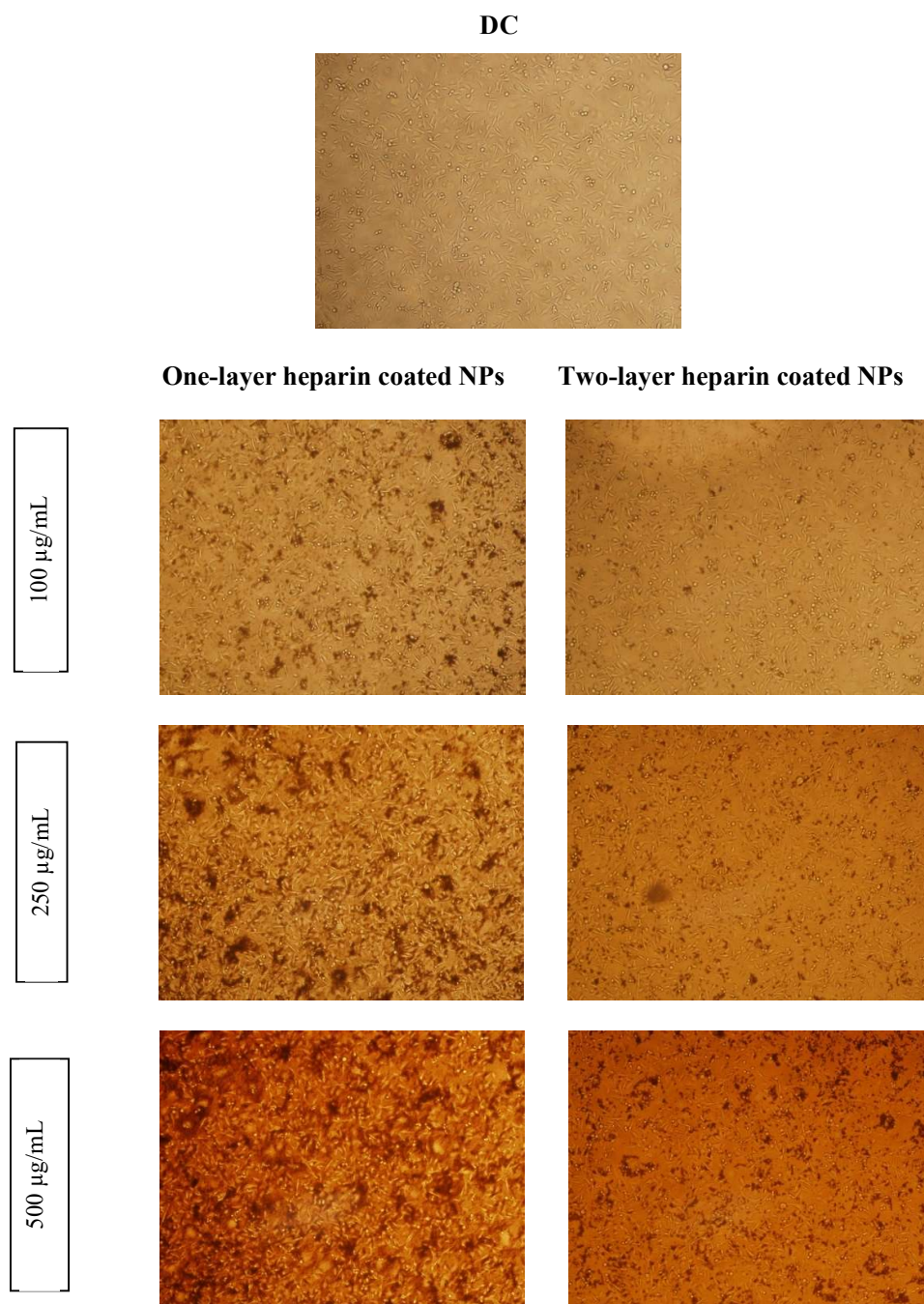


Figure 3.9 Comparison of microscope images of cells treated with one-layer heparin NPs and two-layer heparin NPs

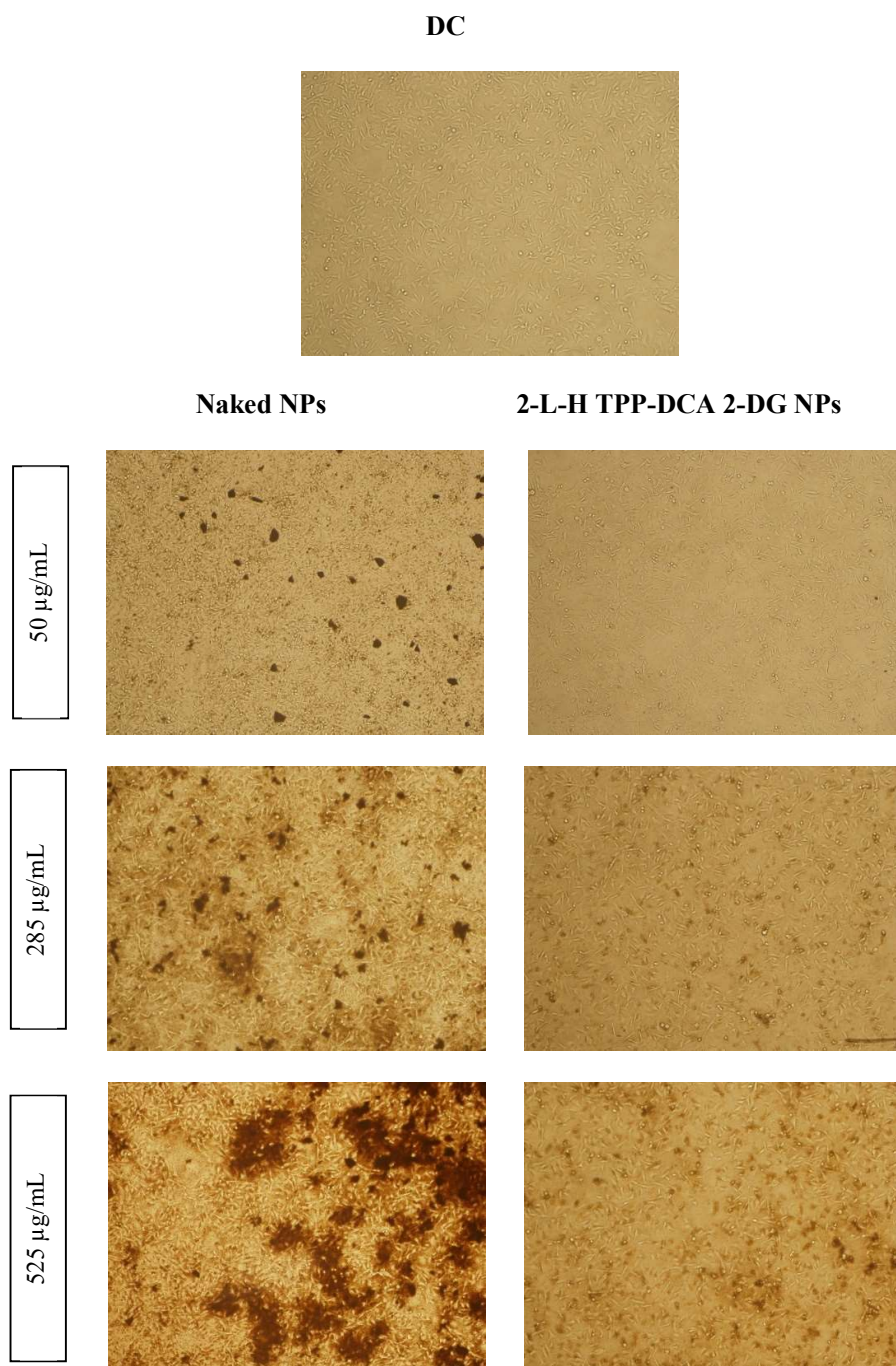


Figure 3.10 Comparison of microscope images of cells treated with naked NPs and two-layer heparin coated TPP-DCA conjugated 2-DG attached NPs.

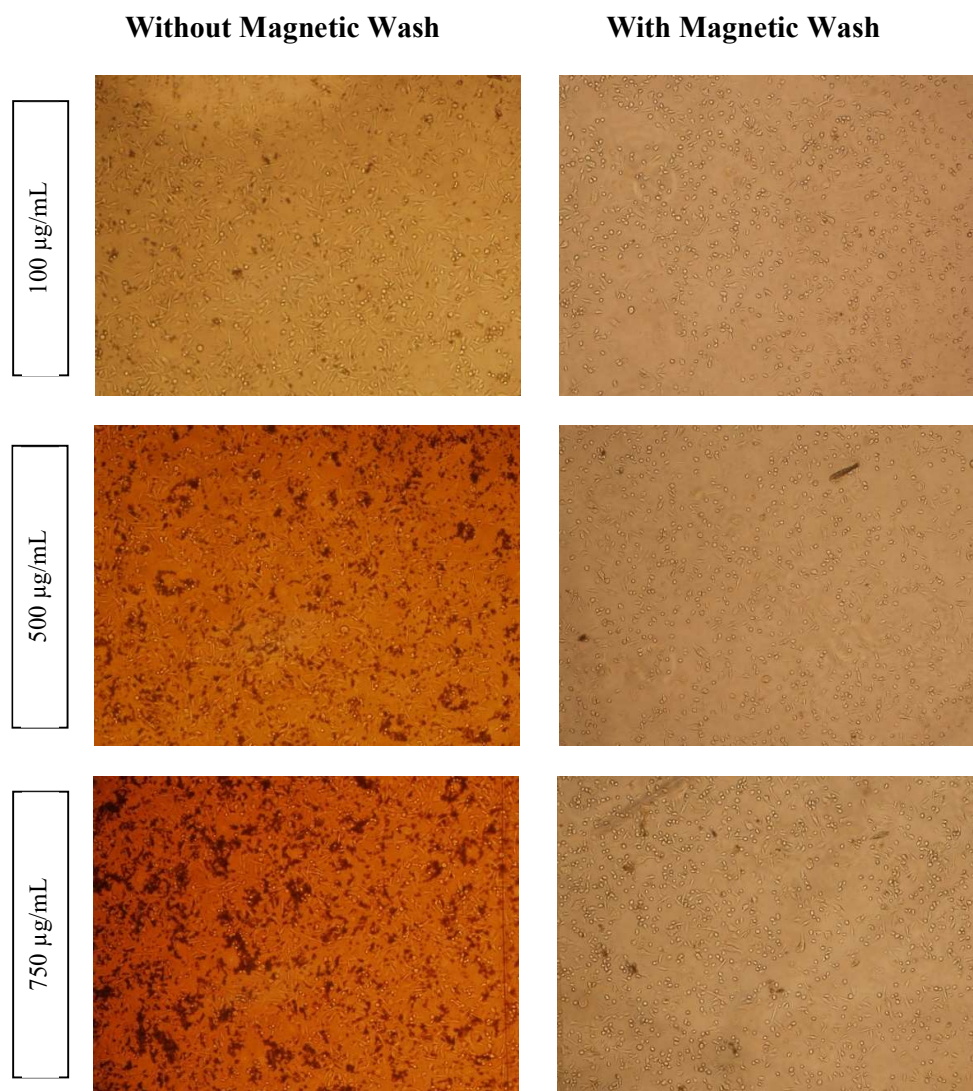
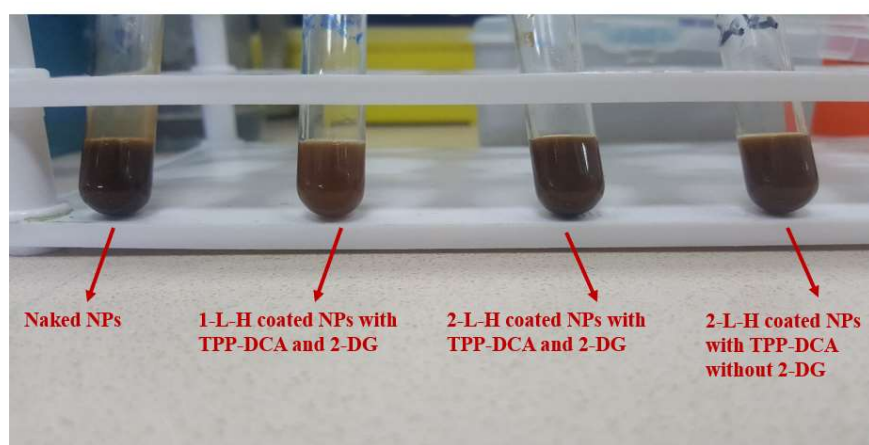


Figure 3.11 Comparison of microscope images of cells treated with two-layer heparin coated TPP-DCA conjugated 2-DG attached NPs with or without magnetic wash.

Moreover, 4 different nanoparticle products were ultra-sonicated (Ultrasonic Cleaner, Alex Machine, Malaysia) for 5 minutes and were kept at room temperature for 15 minutes. As can be seen Figure 3.12, naked nanoparticles were precipitated after 15 minutes whereas heparin-coated nanoparticles were not.

Naked nanoparticles tend to agglomerate by causing the formation of big and nonfunctional molecules, which prevent the cellular uptake. Also, after 24 hr incubation of cells with these nanoparticles, the agglomeration phenomena we mentioned about was observable even with naked eyes (Figure 3.13). More agglomeration was observed in wells containing naked nanoparticles compared to other nanoparticle products containing heparin coating. These results may imply that heparin coating help to increase the solubility of nanoparticles.

(A)



(B)

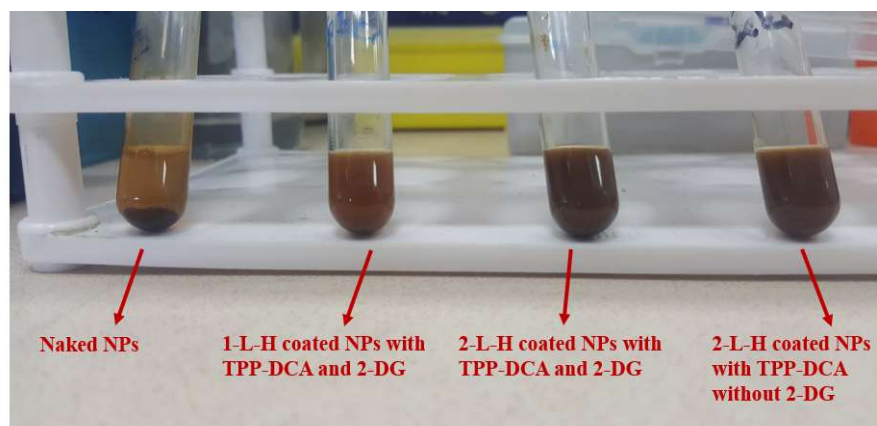


Figure 3.12 Images of 4 different nanoparticle products (A) Immediately after ultra-sonication, (B) 15 minutes after ultra-sonication.

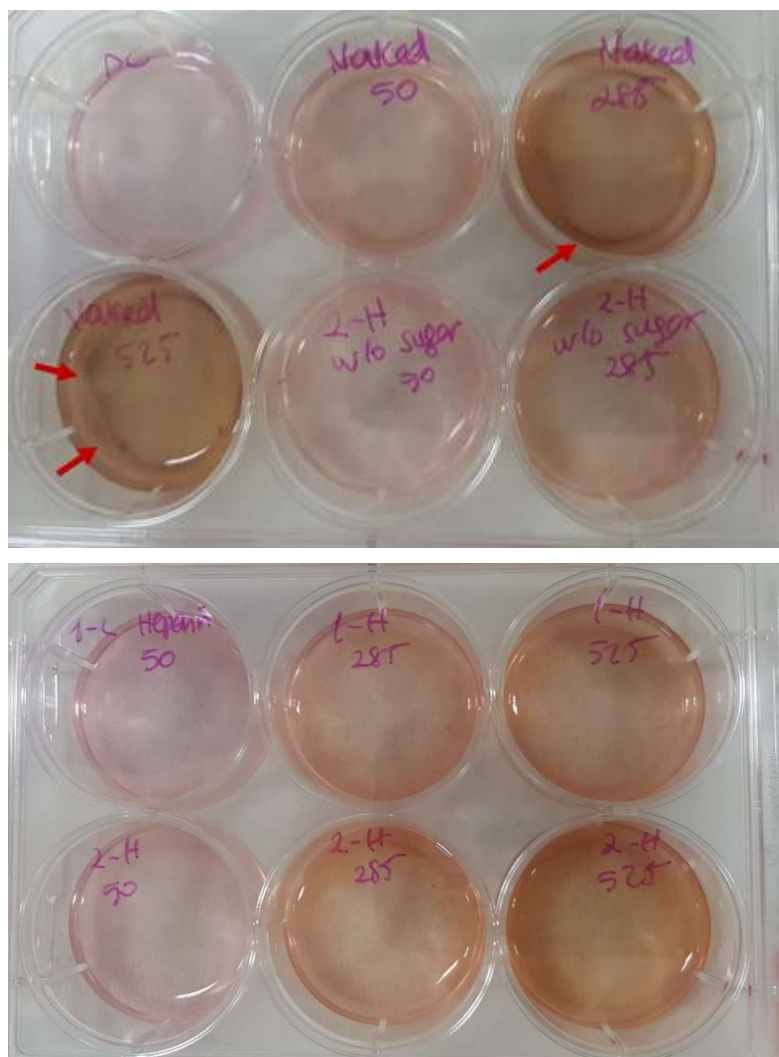


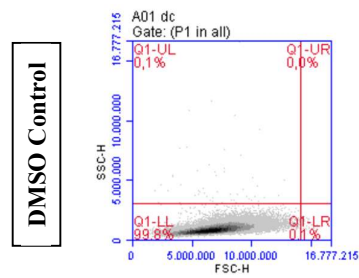
Figure 3.13 Images of wells containing 4 different nanoparticle products after 24-hour treatment before washing.

3.2.3 Determination of Cellular Uptake of Nanoparticles

Cellular uptake of nanoparticles was evaluated in the hepatocellular carcinoma cell line, HepG2, using a flow cytometry. The principle of this assay is based on the differences in the intensity of the scattered light in flow cytometry.

The forward scattered (FSC) light represents cell size while side-scattered (SSC) light represents complexity/granularity of the cell (Suzuki, 2007). The results were shown in Figure 3.14. When results obtained from different nanoparticle treatments were compared, it can be clearly seen that naked nanoparticles had the lowest uptake rate which is 6.4%, 12.1%, and 21.7% for concentrations of 50, 285, and 525 $\mu\text{g/mL}$, respectively compared to other groups. For the same concentrations, cellular uptakes of one-layer heparin coated TPP-DCA conjugated 2-DG attached nanoparticles were 8.6%, 20.3%, and 37.9%, respectively. Also, two-layer heparin coated TPP-DCA conjugated 2-DG attached nanoparticles showed an uptake rate for the same concentrations; 28.6%, 46.2%, and 70.8%. It can be said that as heparin coating increased, cellular uptake of nanoparticles also increased in a dose dependent manner. Moreover, in order to see the effect of 2-D-Glucose on uptake process, we compared cells treated with two-layer heparin coated TPP-DCA conjugated 2-DG attached nanoparticles and those without 2-DG. Nanoparticles without 2-DG showed an uptake rate of 6.5%, 14.8%, and 43.6%, for concentrations of 50, 285, and 525 $\mu\text{g/mL}$ respectively. Presence of 2-DG increased uptake about 27.2% at concentration of 525 $\mu\text{g/mL}$. Also, flow cytometry histograms showing SSC count for different concentrations were shown in Figure 3.15. SSC count for DMSO control (black) was 953.569, while for 285 $\mu\text{g/mL}$ (IC25) (green) it was 2.460.206 and for 525 $\mu\text{g/mL}$, which is the IC50 value (red), it was 3.772.28, showing that, the uptake of our final nanoparticle product into HepG2 cells increased in a dose dependent manner. Hence, according to the results, heparin coating not only helped to increase solubility of nanoparticles, but also it improved their cellular uptake. Also, addition of 2-DG increased the uptake significantly.

A



B

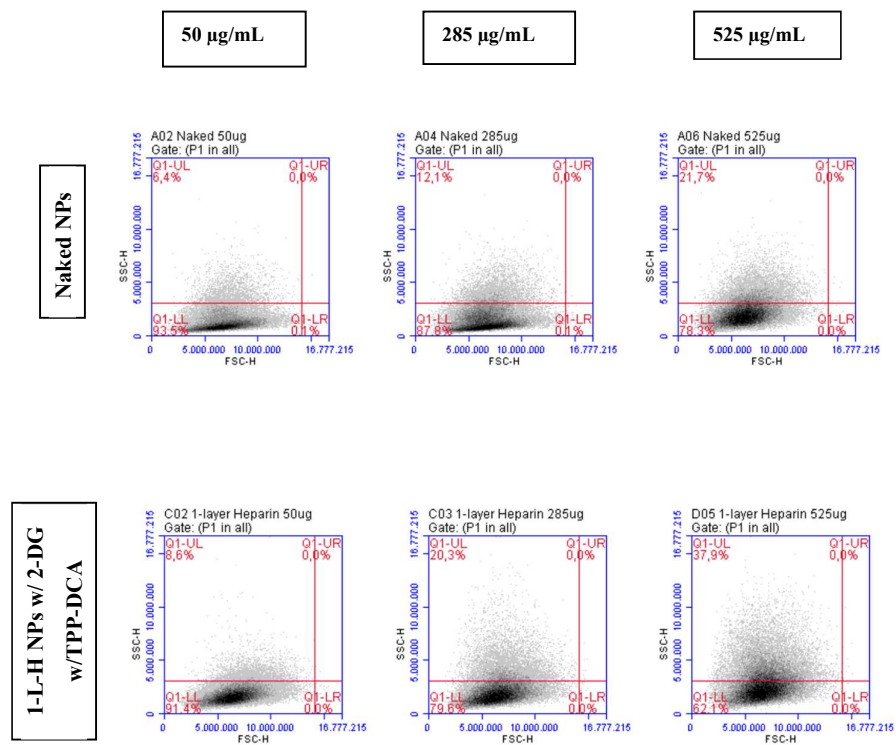


Figure 3.14 Uptake of different nanoparticle products by HepG2 cell line. Real images after treatments with different concentration of NPs (50, 285 and 500 µg/mL) are shown for 24 h and given in the flow cytometry histograms. Cells treated with A) DMSO Control, B) Naked NPs and 1-L-H NPs w/ 2-DG w/TPP-DCA.

C

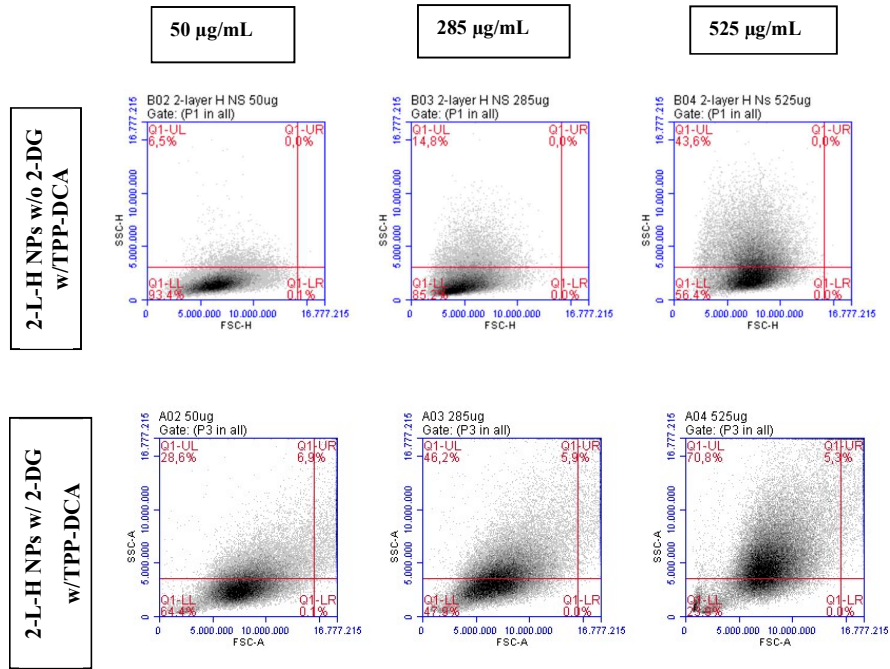


Figure 3.14 (cont') Uptake of different nanoparticle products by HepG2 cell line. Real images after treatments with different concentration of NPs (50, 285 and 500 µg/mL) are shown for 24 h and given in the flow cytometry histograms. Cells treated with C) 2-L-H NPs w/o 2-DG w/TPP-DCA and 2-L-H NPs w/ 2-DG w/TPP-DCA.

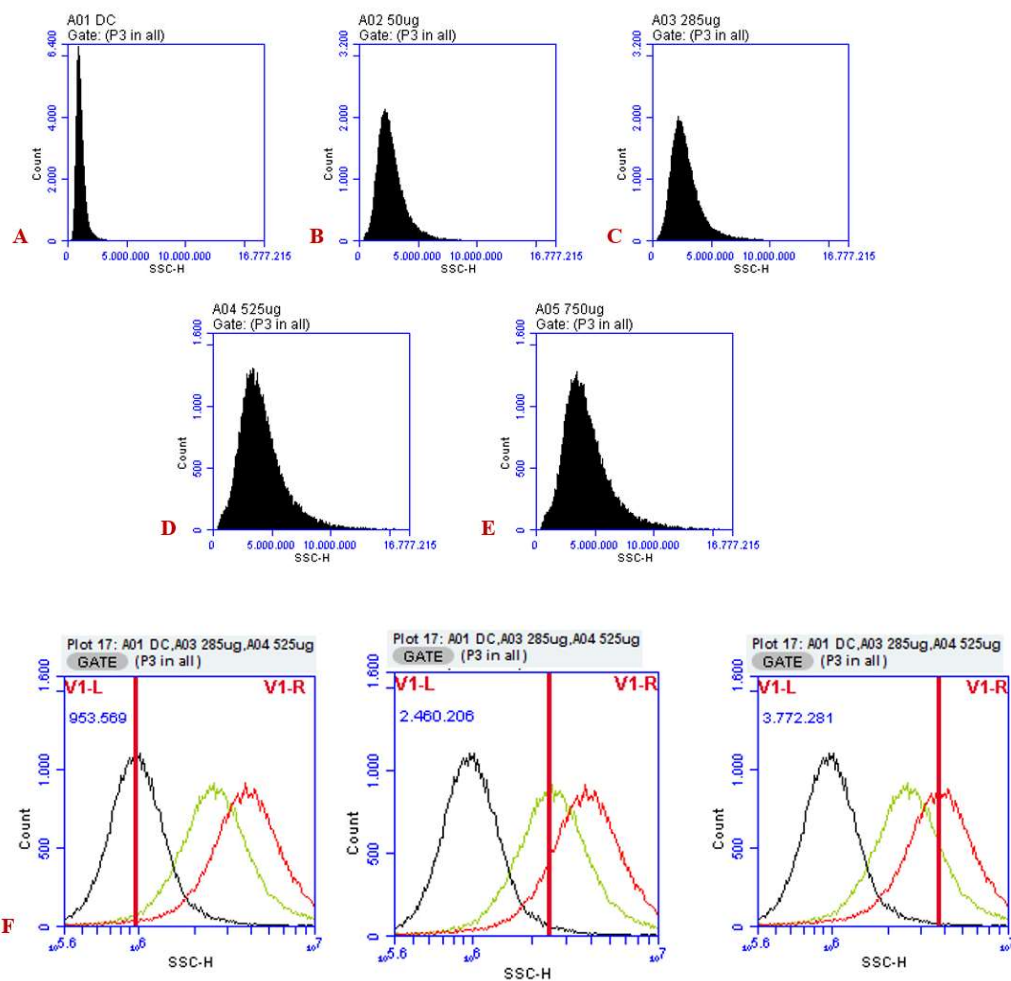


Figure 3.15 (A-E) Separate flow cytometry histograms for cellular uptake of two-layer heparin coated TPP-DCA conjugated 2-DG attached nanoparticles at concentrations of 50, 285, 500, and 750 $\mu\text{g/mL}$. (F) Combined histograms at concentrations of 0 (DC), 285, and 525 $\mu\text{g/mL}$.

3.2.4 Annexin V-FITC Apoptosis Assay

Apoptosis rate was determined by using Annexin V-FITC/PI assay in order to evaluate apoptotic effects of 2-DG-HEP-TPP-DCA-HEP coated IONPs on HepG2 cells upon exposure for 24 hours at concentrations IC₂₅ (285 µg/mL) and IC₅₀ (525 µg/mL). Also, DMSO control (DC) was used as negative control and 50 µM etoposide was used as positive control. Flow cytometry analysis of HepG2 cells performed by using FITC conjugated Annexin-V that is a ligand of phosphatidylserine residue in the plasma membrane and propidium iodide that penetrates disrupted membrane and dyes dead cells. Therefore, cells undergoing apoptosis are observed in FITC⁺ green channel (FL1 channel, A2) in flow cytometry. As the lipid membrane is disrupted, PI that is offered by the kit stains dead cells by penetrating into the cell through disrupted plasma membrane, thus those cells are observed in PI⁺ and FITC⁺ channel (overlap region of FL1 and FL3, A4). The results of this assay are given in Figure 3.16. Most of the cells used for negative control (DC) was in A1 that meant these cells were not stained with any stain (FITC and PI). This result can be explained by that since there was a small amount of apoptotic events as expected, PS residue inner surface of the lipid membrane unlike in apoptotic process, so Annexin-V conjugated with FITC could not bind to it. Also, since plasma membrane were not broken, PI could not penetrate into the plasma membrane, thus cells remained unstained. Therefore, it can be said that unstained cells which was in A1 were thought to be healthy. Cells treated with our final nanoparticle product (2-DG-HEP-TPP-DCA-HEP coated IONPs) at 285 µg/mL (IC₂₅) started to shift towards A2 and A4. Events in A2 shows early-apoptotic cells that translocated their PS to the outside, but their membrane was not destroyed yet. 33.7% of events were in A2 that showed early-apoptotic events, while 1.3% of the events were late apoptotic. When HepG2 cells were treated with nanoparticles (2-DG-HEP-TPP-DCA-HEP coated IONPs) at 525 µg/mL that is IC₅₀ concentration determined in our study for these cells, the total apoptotic events were 69.8% of all population.

Treatment with IC50 concentration caused more apoptotic events compared to negative control. Also, HepG2 cells treated with 50 μ M etoposide for 16 hours which was used as positive control since it is given as IC50 concentration in the literature (Sermeus, 2013), showed 72.6% apoptotic events that 69.8% of the events were in A2 which showed early-apoptotic events and the rest 2.8% were in A4 that showed late-apoptotic ones.

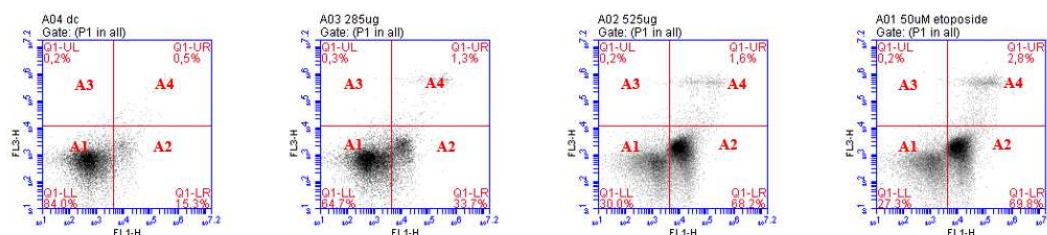


Figure 3.16 The histograms of the apoptotic effects of 2-DG-HEP-TPP-DCA-HEP coated IONPs at concentrations of 285 μ g/mL and 525 μ g/mL on HepG2 cells. Bar graphs show percent apoptotic cells. DMSO control (DC) was used as negative control and 16 hr 50 μ M etoposide exposure was used as positive control. Four subpopulations and their percent distributions in different areas: Area A1 shows viable cells while A3 represents dead cells (necrotic). A2 and A4 correspond to early and late apoptotic events, respectively.

3.2.5 Detection of Mitochondrial Membrane Potential

The changes observed in mitochondrial membrane potential of HepG2 cells in response to NP treatment was determined by using JC-10 Mitochondrial Membrane Potential Assay. In this assay, a reduction in aggregate fluorescent count which refers to depolarization shows green color, whereas an induction which refers to hyperpolarization shows red color in flow cytometry channels.

In healthy cells, JC-10 which is observed as monomers in the cytosol shows green color (Area A2), whereas in the mitochondria it exists mostly as aggregates which is stained as red (Area A1). On the other hand, in dead cells or in the cells undergoing apoptosis, only monomeric form of JC-10 (green) can be observed (Area A1).

Our negative control DMSO showed a clear hyperpolarization in which 97.7% of the cell population exhibited JC-10 in aggregate form which was observed in red color in A1 region, whereas 2.2% of them was in monomeric form (Figure 3.17). Cells treated with 285 $\mu\text{g}/\text{mL}$ of our nanoparticle product (IC25) exhibit a significant shift from A1 to A2 and 31.4% of population showed hyperpolarization, whereas 66.6% of them showed depolarization. When the cells treated with 525 $\mu\text{g}/\text{mL}$ of NPs (IC50), hyperpolarization amount decreased to 21.7%, while depolarization events constituted almost 77.2% of the population. Positive control, when cells treated with 8.7 μM of CCCP which is the IC50 value for HepG2 cells given in literature (Hsu, 2013) showed comparable results with our cells treated with IC50 of NPs. Positive control showed 12.6% hyperpolarization, while 87.4% of the population was found to undergone mitochondrial depolarization.

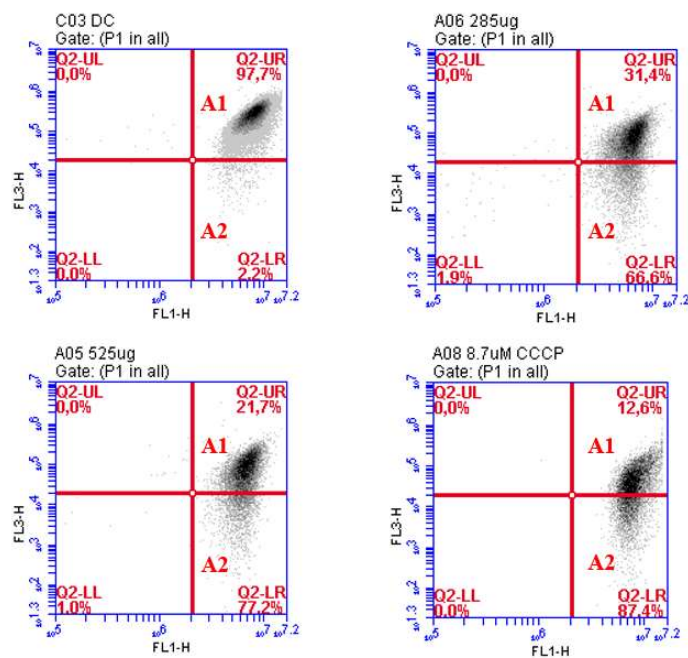


Figure 3.17 The histograms of the mitochondrial membrane potential change in cells treated with 2-DG-HEP-TPP-DCA-HEP coated IONPs at concentrations of 285 $\mu\text{g}/\text{mL}$ and 525 $\mu\text{g}/\text{mL}$ on HepG2 cells. DMSO control (DC) was used as negative control and cells treated with 8.7 μM CCCP were used as positive control. Two subpopulations and their percent distributions in different areas: Area A1 shows hyperpolarization while A2 represents depolarization in mitochondrial membrane.

CHAPTER 4

CONCLUSION

The use of nanotechnology in medicine and more specifically in drug delivery is spreading rapidly. Pharmaceutical sciences use NPs to reduce toxicity and side effects of drugs but carrier systems themselves can have cytotoxic effects on tissues. It is clear that the interaction with tissues and cells, and the potential toxicity, greatly depends on the actual composition of the NP formulation. So, before using these NPs for biomedical applications, we must understand how tailored NPs interact with living systems. Therefore, we studied the cytotoxicity of the tailored nanoparticles in human hepatocellular carcinoma cell line, HepG2.

In this study, in order to increase the cellular uptake of the drug, Dichloroacetate (DCA), iron oxide nanoparticles (Fe_3O_4) were first modified with heparin, DCA is placed inside the heparin layers and in order to use glucose channels, conjugated with 2-deoxy-D-glucose. Triphenylphosphonium (TPP) was also added to induce the uptake by mitochondria.

We found that, heparin coating had a significant effect on solubilization of nanoparticles and second heparin coating increased solubility and consequently uptake of nanoparticles. Moreover, 2-DG conjugation to nanoparticles increased the uptake more than nanoparticles without 2-DG, due to overexpression of GLUT channels in cancer cells as expected.

Our final product, 2-layer heparin coated TPP-DCA conjugated 2-DG attached NPs showed the highest uptake and cytotoxicity in a dose dependent manner and we calculated the IC_{50} value for our tailored nanoparticle as $525 \mu\text{g/mL}$. At this concentration most of the HepG2 cells after 24-hour treatment underwent apoptosis. Furthermore, as the cells were treated with IC_{50} concentration of tailored nanoparticle product, mitochondrial membrane potential was reduced significantly in a dose dependent manner which indicate successful drug delivery.

As a result, our data suggest that nanoparticles engineered to deliver DCA, a chemotherapy agent, by heparin coating TPP-DCA conjugation and 2-DG attachment were successful to deliver the drug of interest. Heparin coating increased solubility, TPP conjugation to DCA increased mitochondrial uptake due to its positively charge and 2-DG increased cellular uptake through GLUT channels which are known to be overexpressed in cancer cells.

For future studies, we are planning to conjugate three DCA molecules to a single TPP molecule instead of one in order to increase the amount of the delivered drug. Also we will use different cancer models and healthy cells in order to see the effect of the tailored nanoparticles for the selective targeting by 2-DG conjugation which we previously found that it increased the cellular uptake in cancer cells (Asik et.al., 2016).

REFERENCES

Akpınar, Y. (2017). *Heparin Coated and 2-Deoxy-D-Glucose Conjugated Iron Oxide Nanoparticles for Biologic Applications*. PhD. Thesis, METU.

Alvarez, J.V., Belka, G.K., Pan, T.C., Chen, C.C., Blankemeyer, E., Alavi, A., Karp, J.S., Chodosh, L.A. (2014). *Oncogene pathway activation in mammary tumors dictates FDG-PET uptake*. *Cancer Res.* 74(24):7583-98.

Asghar, U., Meyer, T. (2012). *Are there opportunities for chemotherapy in the treatment of hepatocellular cancer?* *J Hepatol.* 56(3):686–695.

Asik E., Aslan T.N., Volkan M., Güray N.T. (2016). *2-Amino-2-deoxy-glucose conjugated cobalt ferrite magnetic nanoparticle (2DG-MNP) as a targeting agent for breast cancer cells*. *Environmental Toxicology and Pharmacology.* (41):272–278.

Auffan, M., Decome, L., Rose, J., Orsiere, T., de Meo, M., Briois, V., Chaneac, C., Olivi, L., Berge-Lefranc, J. L., Botta, A., Wiesner, M. R., Bottero, J. W. (2006). *In Vitro interactions between DMSA-coated maghemite nanoparticles and human fibroblasts: a physicochemical and cyto-genotoxic study*. *Environ. Sci. Technol.* 40:4367-4373.

Bava, A., Cappellini, F., Pedretti, E., Rossi, F., Caruso, E., Vismara, E., Gornati, R. (2013). *Heparin and Carboxymethylchitosan Metal Nanoparticles: An Evaluation of Their Cytotoxicity*. *BioMed Research International*, 2013, 314091.

Bava, A., Gornati, R., Cappellini, F., Caldinelli, L., Pollegioni, L., Bernardini, G. (2013). *D-amino acid oxidase-nanoparticle system: a potential novel approach for cancer enzymatic therapy*. *Nanomedicine (Lond)*. 8(11):1797-806.

Bertram, J.S. (2000). *The molecular biology of cancer*. *Mol. Aspects Med.*, 21(6):167-223.

Bonnet, S., Archer, S. L., Allalunis-Turner, J., Haromy, A., Beaulieu, C., Thompson, R., Lee, C. T., Lopaschuk, G. D., Puttagunta, L., Bonnet, S., Harry, G., Hashimoto, K., Porter, C. J., Andrade, M. A., Thebaud, B., Michelakis, E. D. (2007). *A mitochondria-K⁺ channel axis is suppressed in cancer and its normalization promotes apoptosis and inhibits cancer growth*. *Cancer Cell* 11:37–51.

Brunner, T. J., Wick, P., Manser, P., Spohn, P., Grass, R. N., Limbach, L. K., Bruinink, A., Stark, W. J. (2006). *In Vitro Cytotoxicity of oxide nanoparticles: comparison to asbestos, silica, and the effect of particle solubility*. *Environ. Sci. Technol.* 40:4374-4381.

Bull, R.J., Sanchez, I.M., Nelson, M.A., Larson, J.L., Lansing, A.J. (1990). *Liver tumor induction in B6C3F1 mice by dichloroacetate and trichloroacetate*. *Toxicology*. 63(3):341-59.

Cai, X. H., Wang, C. L., Chen, B. A., Hua, W. J., Shen, F., Yu, L., He, Z. M., Shi, Y. Y., Chen, Y., Xia, G. H., Cheng, J., Bao, W., Zhang, Y., Wang, X.M. (2014). *Antitumor efficacy of DMSA modified Fe₃O₄ magnetic nanoparticles combined with arsenic trioxide and adriamycin in raji cells*. *J. Biomed. Nanotechnol.*10:251– 261.

Cao, J., Cui, S., Li, S., Du, C., Tian, J., Wan, S., Qian, Z., Gu, Y., Chen, W.R., Wang, G. (2013). *Targeted cancer therapy with a 2-deoxyglucose-based adriamycin complex*. *Cancer Res.* 73(4):1362-73.

Chen, C.C., Hsieh, D.S., Huang, K.J., Chan, Y.L., Hong, P.D., Yeh, M.K., Wu, C.J. (2014). *Improving anticancer efficacy of (-)-epigallocatechin-3-gallate gold nanoparticles in murine B16F10 melanoma cells*. Drug Design, Development and Therapy. (8):459–474.

Chen, C.L., Chu, J.S., Su, W.C., Huang, S.C., Lee, W.Y. (2010). *Hypoxia and metabolic phenotypes during breast carcinogenesis: expression of HIF-1alpha, GLUT1, and CAIX*. Virchows Arch. 457(1):53-61.

Chen, W., Cao, Y., Liu, M., Zhao, Q., Huang, J., Zhang, H., Deng, Z., Dai, J., Daniel F.B., DeAngelo A.B., Stober J.A., Olson G.R., Page N.P. (1992). *Hepatocarcinogenicity of chloral hydrate, 2-chloroacetaldehyde, and dichloroacetic acid in the male B6C3F1 mouse*. Fundam. Appl. Toxicol. 19(2):159-68.

Darfarin, G., Salehi, R., Alizadeh, E., Nasiri Motlagh, B., Akbarzadeh, A., Farajollahi, A. (2018). *The effect of SiO₂/Au core-shell nanoparticles on breast cancer cell's radiotherapy*. Artif. Cells Nanomed. Biotechnol. 9:1-11.

DeAngelo A.B., George M.H., House D.E. (1999). *Hepatocarcinogenicity in the male B6C3F1 mouse following a lifetime exposure to dichloroacetic acid in the drinking water: dose-response determination and modes of action*. J. Toxicol. Environ. Health A. 58(8):485-507.

DeAngelo A.B., Daniel F.B., Stober J.A., Olson G.R. (1991). *The carcinogenicity of dichloroacetic acid in the male B6C3F1 mouse*. Fundam. Appl. Toxicol. 16(2):337-47.

Deepa, K., Singha, S., Panda, T. (2014). *Doxorubicin nanoconjugates*. J. Nanosci. Nanotechnol. 14(1):892–904.

DiStasio, N., Lehoux, S., Khademhosseini, A., Tabrizian, M. (2018). *The Multifaceted Uses and Therapeutic Advantages of Nanoparticles for Atherosclerosis Research*. Materials (Basel). 11(5).pii:E754.

Eidi, H., Joubert, O., Attik, G., et. Al. (2010). *Cytotoxicity assessment of heparin nanoparticles in NR8383 macrophages*. International Journal of Pharmaceutics. 396(1-2):156–165.

Ekin, A., Karatas, O.F., Culha, M., Ozen, M. (2014). *Designing a gold nanoparticle-based nanocarrier for microRNA transfection into the prostate and breast cancer cells*. J. Gene Med. 16:331–35 4.

Fadok, V.A., Voelker, D.R., Campbell, P.A., Cohen, J.J., Bratton, D.L., Henson, P.M. (1992). *Exposure of phosphatidylserine on the surface of apoptotic lymphocytes triggers specific recognition and removal by macrophages*. J Immunol. 148:2207–2216.

Ferlay, J., Shin, H.R., Bray, F., Forman, D., Mathers, C., Parkin, D.M. (2010). *Estimates of worldwide burden of cancer in 2008: GLOBOCAN 2008*. Int J Cancer 127: 2893–2917.

Fidler, I. J., Kripke, M. L. (2015). *The challenge of targeting metastasis*. Cancer Metastasis Reviews, 34(4), 635–641.

Finichiu, P.G., James, A.M. Larsen, L., Smith, R.A.J. (2013). *Mitochondrial accumulation of a lipophilic cation conjugated to an ionisable group depends on membrane potential, pH gradient and pK_a: implications for the design of mitochondrial probes and therapies*. J. Bioenerg. and Biomembr. 45(1–2):165–173.

Gajalakshmi, P., Priya, M.K., Pradeep, T., Behera, J., Kandasamy, M., Madhuwanti, S., Saran, U., Chatterjee, S. (2013). *Breast cancer drugs dampen vascular functions by interfering with nitric oxide signaling in endothelium*. Toxicol. Appl. Pharmacol. 269:121– 131.

Garg, A., Sharma, R., Pandey, V., Patel, V., Yadav, A.K. (2017). *Heparin-Tailored Biopolymeric Nanocarriers in Site-Specific Delivery: A Systematic Review*. Crit. Rev. Ther. Drug Carrier Syst. 34(1):1-33.

Gewirtz, D.A. (1999). *A critical evaluation of the mechanisms of action proposed for the antitumor effects of the anthracycline antibiotics adriamycin and daunorubicin*. Biochem Pharmacol. 57(7):727-41.

Gupta, A.K., Gupta, M. (2005). *Cytotoxicity suppression and cellular uptake enhancement of surface modified magnetic nanoparticles*. Biomaterials. 26:1565-1573.

Haddad, P.S., Seabra, A.B. (2012). *Biomedical Applications of Magnetic Nanoparticles*, in Iron Oxides: Structure, Properties and Applications (Martinez, A. I., Ed.) 1st ed., 1:165– 188, Nova Science Publishers, Inc., New York.

Herren-Freund S.L., Pereira M.A., Khoury M.D., Olson G. (1987). *The carcinogenicity of trichloroethylene and its metabolites, trichloroacetic acid and dichloroacetic acid, in mouse liver*. Toxicol. Appl. Pharmacol. 90(2):183-9.

Hsu, C.C., Wang, C.H., Wu, L.C., Hsia, C.Y., Chi, C.W., Yin, P.H., Chang, C.J., Sung, M.T., Wei, Y.H., Lu, S.H., Lee, H.C. (2013). *Mitochondrial dysfunction represses HIF-1 α protein synthesis through AMPK activation in human hepatoma HepG2 cells.* Biochim. Biophys. Acta. 1830(10):4743-51.

Iv, M., Telischak, N., Feng, D., Holdsworth, S.J., Yeom, K.W., Daldrup-Link, H.E. (2015). *Clinical applications of iron oxide nanoparticles for magnetic resonance imaging of brain tumors.* Nanomedicine. 10:993–1018.

Jayant, R.D., Gupta, P., Garcia, E., Sarkar, A., Kapoor, S., Rafiq, K., Chand, H.S., Nair, M. (2018). *Nanoparticle based treatment for Cardiovascular Diseases.* Cardiovasc. Hematol. Disor. Drug Targets.

Jemal, A., Bray, F., Center, M.M., Ferlay, J., Ward, E., Forman, D. (2011). *Global cancer statistics.* CA Cancer J Clin 61: 69–90.

Jian, W., Lai, K. L., Wu, Y., Gu, Z. W. (2014). *Protein corona on magnetite nanoparticles and internalization of nanoparticle-protein complexes into healthy and cancer cells.* Arch. Pharm. Res. 37:129-141.

Jong, W.H.D., Borm, P.J.A. (2008). *Drug delivery and nanoparticles: Applications and hazards.* Int. J. Nanomedicine. 3(2): 133–149.

Kalyanaraman, B. (2017). *Teaching the basics of cancer metabolism: Developing antitumor strategies by exploiting the differences between normal and cancer cell metabolism.* Redox Biology, 12:833–842.

Kankotia, S., Stacpoole, P.W. (2014). *Dichloroacetate and cancer: new home for an orphan drug?* Biochim. Biophys. Acta. 1846(2):617-29.

Karlsson, J., Vaughan, H.J., Gren, J.J. (2018). *Biodegradable Polymeric Nanoparticles for Therapeutic Cancer Treatments*. *Annu. Rev. Chem. Biomol. Eng.* 9:6.1–6.23.

Kato, M., Li, J., Chuang, J.L., Chuang, D.T. (2007). *Distinct structural mechanisms for inhibition of pyruvate dehydrogenase kinase isoforms by AZD7545, dichloroacetate, and radicicol*. *Structure*, 15:992-1004.

Kemp, M.M., Linhardt, R.J. (2010). *Heparin-based nanoparticles*. *Wiley Interdisciplinary Reviews: Nanomedicine and Nanobiotechnology*. 2(1):77–87.

Kesavan, M.P., Kotla, N.G., Ayyanaar, S., Kumar, G.G.V., Rajagopal, G., Sivaraman, G., Webster, T.J., Rajesh, J. (2018). *A theranostic nanocomposite system based on iron oxide-drug nanocages for targeted magnetic field responsive chemotherapy*. *Nanomedicine*. S1549-9634(18)30085-6.

Koban, I., Matthes, R., Hübner, N.-O., Welk, A., Sietmann, R., Lademann, J., Kocher, T. (2012). *XTT assay of ex vivo saliva biofilms to test antimicrobial influences*. *GMS Krankenhaushygiene Interdisziplinär*, 7(1).

Koppenol, W.H., Bounds, P.L., Dang, C.V. (2011). *Otto Warburg's contributions to current concepts of cancer metabolism*. *Nat. Rev. Cancer*. 11(5):325-37.

Lin, K.Y., Kwon, E.J., Lo, J.H., Bhatia, S.N. (2014). *Drug-induced amplification of nanoparticle targeting to tumors*. *Nano Today*. 9(5):550-559.

Lin, Z., Zheng, J., Lin, F., Zhang, L., Caic, Z., Chen, G. (2011). *Synthesis of magnetic nanoparticles with immobilized aminophenylboronic acid for selective capture of glycoproteins*. *J. Mater. Chem.* 21, 518-524.

Liu, C.Y., Chen, K.F., Chen, P.J. (2015). *Treatment of Liver Cancer*. Cold Spring Harbor Perspectives in Medicine, 5(9).

Liu, L., Cao, Y., Chen, C., Zhang, X., McNabola, A., Wilkie, D., Wilhelm, S., Lynch, M., Carter, C. (2006). *Sorafenib blocks the RAF/MEK/ERK pathway, inhibits tumor angiogenesis, and induces tumor cell apoptosis in hepatocellular carcinoma model PLC/PRF/5*. Cancer Res 66: 11851–11858.

Liu, Y., Miyoshi, H., Nakamura, M. (2007). *Nanomedicine for drug delivery and imaging: A promising avenue for cancer therapy and diagnosis using targeted functional nanoparticles*. Int. J. Cancer, 120:2527-2537.

Madhusudhan, A., Reddy, G.B., Venkatesham, M., Veerabhadram, G., Kumar, D.A., et al. (2014). *Efficient pH dependent drug delivery to target cancer cells by gold nanoparticles capped with carboxymethyl chitosan*. Int. J. Mol. Sci. 15:8216–34.

Malekzad, H., Zangabad, P.S., Mohammadi, H., Sadroddini, M., Jafari, Z., Mahlooji, N., Abbaspour, S., Gholami, S., Ghanbarpoor, M., Pashazadeh, R., Beyzavi A., Karimi, M., Hamblin M.R. (2018). *Noble metal nanostructures in optical biosensors: Basics, ant their introduction to anti-doping detection*. Trends Analt. Chem. 100:116-135.

Michelakis, E.D., Webster, L., Mackey, J.R. (2008). *Dichloroacetate (DCA) as A Potential Metabolic-Targeting Therapy for Cancer*. Br. J. Cancer, 99:989–994.

Mora-Huertas, C.E., Fessi, H., Elaissari, A. (2010). *Polymer-based nanocapsules for drug delivery*. International Journal of Pharmaceutics. 385(1-2):113–142.

Mueckler, M., Thorens, B. (2013). *The SLC2 (GLUT) family of membrane transporters*. Mol Aspects Med. 34(2-3):121-38.

Muley, P., Olinger, A., Tummala, H. (2015). *2-Deoxyglucose induces cell cycle arrest and apoptosis in colorectal cancer cells independent of its glycolysis inhibition*. *Nutr. Cancer*. 67(3):514-522.

Murphy, M.P., Smith, R.A.J. (2007). *Targeting Antioxidants to Mitochondria by Conjugation to Lipophilic Cations*. *Annu. Rev. Pharmacol. Toxicol.*, 47:629-656.

Nazir, S., Hussain, T., Ayub, A., Rashid, U., MacRobert, A. J. (2014). *Nanomaterials in combating cancer: Therapeutic applications and developments*. *Nanomed. Nanotechnol.* 10:19– 34.

Neveu, M.A., Preter, G.D., Joudiou, N., Bol, A., Brender, J.R., Saito, K., Gallez, B. (2016). *Multi-modality imaging to assess metabolic response to dichloroacetate treatment in tumor models*. *Oncotarget*. 7(49):81741–81749.

Pathak, R.K., Marrache, S., Harn, D.A., Dhar, S. (2014). *Mito-DCA: A Mitochondria Targeted Molecular Scaffold for Efficacious Delivery of Metabolic Modulator Dichloroacetate*. *ACS Chem. Biol.* 9:1178–1187.

Pelicano, H., Martin, D.S., Xu, R.H., Huang, P. (2006). *Glycolysis inhibition for anticancer treatment*. *Oncogene*. 25(34):4633-46.

Pereira, M.A. (1996). *Carcinogenic activity of dichloroacetic acid and trichloroacetic acid in the liver of female B6C3F1 mice*. *Fundam. Appl. Toxicol.* 31(2):192-9.

Perry, S.W., Norman, J.P., Barbieri, J., Brown, E.B., Gelbard, H.A. (2011). *Mitochondrial membrane potential probes and the proton gradient: a practical usage guide*. *BioTechniques*, 50(2):98–115.

Roberts, D.J., Miyamoto, S. (2015). *Hexokinase II integrates energy metabolism and cellular protection: acting on mitochondria and TORCing to autophagy*. *Cell Death Differ.* 22(2):248-257.

Roche, T.E., Baker, J.C., Yan, X., Hiromasa, Y., Gong, X., Peng, T., Dong, J., Ruggiero, C., Pastorino, L., Herrera, O.L. (2010). *Nanotechnology based targeted drug delivery*. *Conf. Proc. IEEE Eng. Med. Biol. Soc.* 2010:3731-2.

Schoonen, L., van Hest, J.C. (2014). *Functionalization of protein-based nanocages for drug delivery applications*. *Nanoscale*. 6(13):7124-41.

Seabra, A. B., Duran, N. (2013). *Biological applications of peptides nanotubes: An overview*. *Peptides*. 39:47– 54.

Seabra, A.B., Pasquôto, T., Ferrarini, A.C.F., Cruz Santos, M., Haddad, P.S., Lima, R. (2014). *Preparation, Characterization, Cytotoxicity, and Genotoxicity Evaluations of Thiolated- and S-Nitrosated Superparamagnetic Iron Oxide Nanoparticles: Implications for Cancer Treatment*. *Chem. Res. Toxicol.* 27 (7):1207–1218.

Sermeus, A., Rebutti, M., Fransolet, M., Flamant, L., Desmet, D., Delaive, E., Arnould, T., Michiels, C. (2013). *Differential Effect of Hypoxia on Etoposide-Induced DNA Damage Response and p53 Regulation in Different Cell Types*. *J. Cell. Physiol.* 228:2365-2376.

Shi, J., Votruba, A.R., Farokhzad, O.C., Langer, R. (2010). *Nanotechnology in Drug Delivery and Tissue Engineering: From Discovery to Applications*. Nano Lett., 10(9):3223-3230.

Shyam, K., Stacpoole, P.W. (2014). *Dichloroacetate and cancer: New home for an orphan drug?* Biochimica et Biophysica Acta, 1846:617–629.

Siegel, R.L. (2018). *Cancer Facts & Figures 2018*. CA Cancer Journal for Clinicians. American Cancer Society.

Siegel, R.L. (2018). *Cancer Statistics, 2018*. CA Cancer Journal for Clinicians. American Cancer Society.

Singh, R., Lillard, G.W.G. (2009). *Nanoparticle-based targeted drug delivery*. Exp. Mol. Pathology. 86:215-223.

Singh, S., Nalwa, H.S. (2007). *Nanotechnology and health safety--toxicity and risk assessments of nanostructured materials on human health*. J Nanosci Nanotechnol. 7(9):3048-70.

Stacpoole, P.W. (1989). *The pharmacology of dichloroacetate*. Metabolism. 38(11):1124-44.

Stacpoole, P.W., Felts, J.M. (1970). *Diisopropylammonium dichloroacetate (DIPA) and sodium dichloroacetate (DCA): effect on glucose and fat metabolism in normal and diabetic tissue*. Metabolism, 19 (1970), pp. 71-78.

Stacpoole, P.W., Gilbert, L.R., Neiberger, R.E., Carney, P.R., Valenstein, E., Su, L., Zhang, H., Yan, C., Chen, A., Meng, G., Wei, J., Ding, Y. (2016). *Superior anti-tumor efficacy of diisopropylamine dichloroacetate compared with dichloroacetate in a subcutaneous transplantation breast tumor model*. *Oncotarget*, 7(40):65721–65731.

Suzuki, H., Toyooka, T., Ibuki, Y. (2007). *Simple and easy method to evaluate uptake potential of nanoparticles in mammalian cells using a flow cytometric light scatter analysis*. *Environmental science & technology*. 41:3018-3024.

Theriaque, D.W., Shuster, J.J. (2008). *Evaluation of long-term treatment of children with congenital lactic acidosis with dichloroacetate*. *Pediatrics*, 121, pp. e1223-e1228

Truffi, M., Colombo, M., Sorrentino, L., Pandolfi, L., Mazzucchelli, S., Pappalardo, F., Pacini, C., Allevi, R., Bonizzi, A., Corsi, F., Prospero, D. (2018). *Multivalent exposure of trastuzumab on iron oxide nanoparticles improves antitumor potential and reduces resistance in HER2-positive breast cancer cells*. *Sci. Rep.* 8(1):6563.

Turkan, A., Kasten, S.A. (2001). *Distinct regulatory properties of pyruvate dehydrogenase kinase and phosphatase isoforms*. *Prog. Nucleic Acid Res. Mol. Biol.*, 70:33-75.

van Engeland, M., Nieland, L.J., Ramaekers, F.C., Schutte, B., Reutelingsperger, C.P. (1998). *Annexin V-affinity assay: a review on an apoptosis detection system based on phosphatidylserine exposure*. *Cytometry*. 31:1–9.

Venturelli, L., Nappini, S., Bulfoni, M., Gianfranceschi, G., Dal Zilio, S., Coceano, G., Cojoc, D. (2016). *Glucose is a key driver for GLUT1-mediated nanoparticles internalization in breast cancer cells*. *Scientific Reports*. 6:21629.

Wahajuddin, Arora, S. (2012). *Superparamagnetic iron oxide nanoparticles: magnetic nanoplatforms as drug carriers*. Int. J. Nanomedicine. 7:3445-3471.

Wang, S.Y., Wei, Y.H., Shieh, D.B. et.al. (2015). *2-Deoxy-D-Glucose can complement doxorubicin and sorafenib to suppress the growth of papillary thyroid carcinoma cells*. PLoS One.10(7):e0130959

Williams, D. F., Zhang, Z. (2012). *Rotavirus capsid surface protein VP4-coated Fe₃O₄ nanoparticles as a theranostic platform for cellular imaging and drug delivery*. Biomaterials 33:7895– 7902.

Wilson, J.W., Potten, C.S. (2005). *Cell turnover: intestine and other tissues*, in When Cells Die II, a Comprehensive Evaluation of Apoptosis and Programmed Cell Death (by Lockshin RA and Zakeri Zeds). John Wiley & Sons. pp 201–240.

Xiong, F., Zhu, Z.Y., Xiong, C., Hua, X.Q., Shan, X.H., Zhang, Y., Gu, N. (2012). *Preparation, Characterization of 2-Deoxy-D-Glucose Functionalized Dimercaptosuccinic Acid-Coated Maghemite Nanoparticles for Targeting Tumor Cells*. Pharm. Res. 29(4):1087-97.

Yu, C., Zhao, J., Guo, Y., Lu, C., Ma, X., Gu, Z. (2008). *A novel method to prepare water-dispersible magnetic nanoparticles and their biomedical applications: magnetic capture probe and specific cellular uptake*. J. Biomed. Mater. Res. A. 87(2):364-72.

Zhang, N., Palmer, A.F. (2011). *Development of a dichloroacetic acid-hemoglobin conjugate as a potential targeted anti-cancer therapeutic*. Biotechnol. Bioeng. 108(6):1413-20.

Zhao, M., Liu, M. (2018). *New Avenues for Nanoparticle-Related Therapies*. *Nanoscale Res. Lett.* 13(1):136.

Zhao, X., Chen, Q., Liu, W., Li, Y., Tang, H., Liu, X., Yang, X. (2015). *Codelivery of doxorubicin and curcumin with lipid nanoparticles results in improved efficacy of chemotherapy in liver cancer*. *International Journal of Nanomedicine*, 10, 257–270.

Zhou, J., Zhang, J., Gao, W. (2014). *Enhanced and selective delivery of enzyme therapy to 9L-glioma tumor via magnetic targeting of PEG-modified, beta-glucosidase-conjugated iron oxide nanoparticles*. *Int. J. Nanomed.* 9:2905–17.

Zhu, J., Zheng, L., Wen, S., Tang, Y., Shen, M. et al. (2014). *Targeted cancer theranostics using alphotocopheryl succinate-conjugated multifunctional dendrimer-entrapped gold nanoparticles*. *Biomaterials* 35:7635–46.